Colloids and Surfaces A: Physicochemical and Engineering Aspects 737 (2026) 139961

Contents lists available at ScienceDirect

Colloids and Surfaces A: Physicochemical and Engineering Aspects

journal homepage: www.elsevier.com/locate/colsurfa

Polyethylene nanoplastic-protein interactions assessed via corona adsorption isotherms from Small-Angle X-ray Scattering (SAXS)

Thomas Perrault [a], Léa Jacquin [b], Marion Schvartz [a,c], Florent Saudrais [c], Aurélien Thureau [d], Vincent Monteil [b], Serge Pin [c], Yves Boulard [e], Jean-Philippe Renault [c], Fabrice Brunel [b], Guillaume Brotons [a,*]

[a] Institute of Molecules and Materials of Le Mans (IMMM), UMR 6283, Le Mans, France
[b] University of Claude Bernard Lyon 1, CNRS, CPE Lyon, UMR 5128, Laboratory of Catalysis, Polymerization, Processes and Materials (CP2M), 43 Bd du 11 Nov. 1918, Villeurbanne, France
[c] University of Paris-Saclay, CEA, CNRS, NIMBE, LIONS, Gif-sur-Yvette, 91191, France
[d] Synchrotron SOLEIL, L'Orme des Merisiers, Départementale 128, Saint-Aubin, 91190, France
[e] University of Paris-Saclay, CEA, CNRS, Institute for Integrative Biology of the Cell (I2BC), Gif-sur-Yvette, 91198, France

GRAPHICAL ABSTRACT

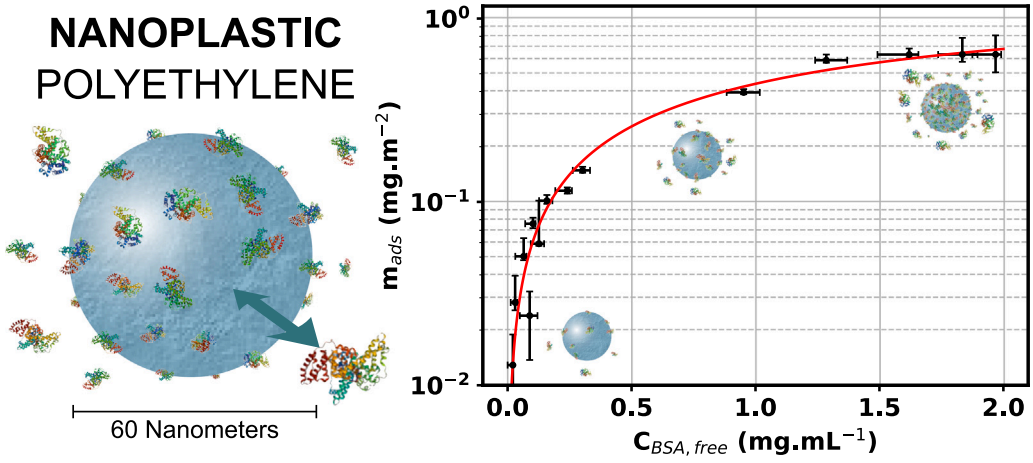

HIGHLIGHTS

- Smallest PE fragments, most abundant plastic pollutants, cover with proteins in water.
- Nanoplastic surfaces and proteins conformational remodeling, control their affinity.
- Corona protein adsorption isotherms on nanoplastics, built via in-situ SAXS analysis.
- BSA dense Langmuir monolayers form on pristine polyethylene nano and micro plastics.
- Preparation of polyethylene nanoplastics with a well-controlled BSA protein corona.

ARTICLE INFO

Keywords:

ABSTRACT

* Corresponding author.
E-mail addresses: thomas.perrault@univ-lemans.fr (T. Perrault), guillaume.brotons@univ-lemans.fr (G. Brotons).

https://doi.org/10.1016/j.colsurfa.2026.139961
Received 8 December 2025; Received in revised form 20 January 2026; Accepted 11 February 2026
Available online 12 February 2026

Micro and nanoplastics (MNPs)
Polyethylene (PE) environmental fate
Protein corona
Langmuir isotherm
Small-Angle X-ray scattering (SAXS)

The spontaneous formation of a model protein corona was studied on nanoplastics, considered as model nanoparticles of the smallest fragments resulting from polyethylene (PE-NPs), which is the most abundant plastic environmental pollutant. Well-individualized monomeric BSA proteins and 30 nm radius PE-NPs, were mixed at different concentration ratios in a phosphate buffer and studied using Small-Angle X-ray Scattering (SAXS) experiments. The average number of proteins adsorbed per particle, their hydration, as well as the concentration of free proteins remaining in solution is measured by fitting the whole SAXS data in absolute scale of the intensity [cm^{-1}] over a large q-range. In this way, protein adsorption isotherms were built and show a good agreement with the Langmuir monolayer model. We found a higher affinity in the case of pristine PE-NPs (3.15 $L.g^{-1}$) compared to PE-NPs stabilized with traces of pegylated surfactants (0.41 $L.g^{-1}$), in line with previously reported values for nanoparticles of a different nature such as SiO_2 or polystyrene (PS). The protein affinity depends on the PE particle size and surface state. At physiological pH, a dense BSA corona formed on pristine PE-NPs with a maximum amount of adsorbed proteins at the monolayer's saturation of 1.5 $mg.m^{-2}$, that compares well to pristine PE microplastic measurements. Such tailored and stable PE-NPs with a controlled protein corona are suitable for a wide range of applications, including the study of their fate in biotic and abiotic environments.

1. Introduction

Plastics have become omnipresent in our society due to their numerous benefits such as affordability, lightweight nature, and ease of manufacturing. However, worldwide, fewer than 10% of plastics are recycled, and over 30% of them leak into the environment, which has become a major societal concern [1,2]. Following their photodegradation, they are progressively fragmented into micro/nano-plastics (MNPs) which are easily integrated into the food chain with possible toxic effects [3]. It is worth noting that most of the reported toxicological studies were conducted using polystyrene due to its ease in synthesis and/or processing into nanoparticles (NPs), while the most common commercial used of commercial plastics are polyolefins (*e.g.*, polyethylene and polypropylene) [4]. Among the smallest particulate fragments produced in the environment or for conducting model experiments, nanoplastics (NP) have the highest surface-to-volume ratio, which gives their surface charges a predominant role in terms of both their stability in water [5] and their interactions with environmental molecules [6]. Recently, we developed a unique free radical emulsion polymerization of ethylene in aqueous media under mild conditions (temperature < 90 ° C and ethylene pressure < 250 bar) yielding stable and narrowly distributed polyethylene (PE) nanoparticles [7,8], which are well suited to study the impact of PE-NPs in the environment. Furthermore, in order to produce environmentally realistic PE-NPs, it is important to coat them with specific biomolecules, forming an eco-corona, which plays a critical role in the fate of nanoparticles within biological systems, influencing their pharmacokinetics, biodistribution, and cellular interactions [9]. The eco-corona layer formed around NPs is composed of various biochemical constituents, typically comprising cellular polymeric substances (such as DNA, proteins, and carbohydrates) and humic substances (such as humic acid, fulvic acid, and humin), which are excreted by organisms or arise from the degradation of organic matter [6,10]. Understanding the formation and characteristics of the protein corona on PE-NPs is therefore of paramount importance.

In recent years, advances in structural and analytical techniques, such as Small Angle X-ray or Neutron Scattering (SAXS and SANS, respectively), have provided valuable insights into the structure and nature of protein coronas on nanoparticles, when enough scattering contrast between materials is reached and quantitative estimations are made. Many of the studies on the interaction of model proteins with nano and micro-particles in aqueous solutions are carried out using inorganic and metallic colloids including SiO_2, TiO_2, Au or polystyrene nanoparticles [11–18]. Likewise, one of the most widely used protein model in biochemical assays is Bovine Serum Albumin (BSA, ≈66.5 kDa), an analogue of Human Serum Albumin (HSA, ≈66.5–66.8 kDa), with similar structure and function such as maintaining osmotic pressure, pH buffering, and transporting ligands. All of these studies highlight the complex nature of the corona formation, as many factors must be considered including pH, salts, concentrations, sizes or zeta-potentials.

In this study, we delve into the structure of the protein corona using a model in-situ contact experiment, based on the interaction of well-known bovine serum albumin (BSA) proteins with monodisperse PE-NPs synthesized *via* an emulsion polymerization process to control their chemical composition, surface state (often unknown for commercially available NPs or MPs), and size distribution. We varied the concentration ratios of both PE-NPs and BSA to gain a comprehensive understanding of the corona formation with respect to thermodynamical adsorption constants that rule a dynamical exchange processes of adsorbed BSA in equilibrium with free bulk proteins. The approach we followed is similar to Ref. [19] where the authors studied the adsorption of BSA on negatively charged SiO_2 nanoparticles, varying similar ratio following the so-called Job's plot method, which consists of monitoring the interactions between NPs and proteins by measuring characteristic sizes when varying the molar concentration of NPs and proteins and keeping the total concentration constant. The authors did not observe a clear BSA corona formation onto SiO_2 with SAXS experiments, probably due to the huge contrast between SiO_2 and water, so the BSA shell-layer between the silica and the solvent is practically undetectable. Similarly, Han et al. [20] performed SAXS experiments, along with dynamic light scattering (DLS) experiments, on SiO_2/BSA mixtures to study the corona formation and aggregation. The BSA corona formation was detected from DLS measurements but hard to see by SAXS for the same reason. Here, thanks to the low electron density of PE compared with SiO_2, we obtained enough scattering contrast to detect the BSA corona shell forming between the PE-NPs core and the solution. Our quantitative SAXS analysis also significantly benefits from the small size and narrow size distribution of both our model particles and proteins.

2. Materials and methods

2.1. Chemicals and materials

Bovine serum albumin (BSA), ammonium persulfate (APS) and sodium hydrogencarbonate ($NaHCO_3$, used in the synthesis) were purchased from Sigma Aldrich. 2,2'-Azobis[2-methyl-N-(2-hydroxyethyl) propionamide] (VA-086) and Disponil A 3065 (DSP), a modified ethoxylates of native fatty alcohols: PEG chains -$(OCH_2CH_2)_{30}OH$ bounded to -$C_{12}H_{25}$ alkyl chains, were purchased from Wako Fujifilm and Cognis, respectively. Solutions were based on Milli-Q water, phosphate buffer (PB) made by mixture of: $Na_2HPO_4 \cdot 2H_2O$ and $NaH_2PO_4 \cdot 2H_2O$ purchased from VWR Chemicals. All dialysis were performed using pre-wetted and thoroughly washed low nonspecific protein interaction dialysis membrane of 3.5 kDa (purchased from Spectra-Por).

2.2. Preparation of PE-NP

PE-NPs were synthesized following the procedure outlined in Refs. [7,8,21], using a free radical emulsion polymerization approach. Basically, the principle consists in polymerizing gaseous ethylene monomers using an initiator in aqueous solution in a specialized stainless steel reactor designed for this dangerous reaction. The initiator used for this process is VA-086 in conjunction with DSP surfactants or APS in surfactant-free aqueous solution. During the polymerization process, since VA-086 is a neutral initiator, addition of DSP is needed to ensure the NPs stabilization, while in the case of APS, which is an anionic initiator (sulfate groups, SO_3^-), the stabilization is ensured by electrostatic interactions so that no surfactant is needed in the aqueous solutions. The polymerization reaction occurs by introducing ethylene gas into the solution containing the initiator in a reactor at specific temperature (T), pH, ethylene pressure (P_{ethylene}) and stirring rate (SR) for 4 h. By tuning these parameters continuously, the yield (polymer content, PC [%w/w]), particle size distribution (function $p_z(R)$) and molar mass [g/mol] will differ. The synthesis conditions of the surfactant-built nanoparticle batch sample are the same concentration of VA-086 and DSP at 0.2%w/w, 100 bar of ethylene pressure, a temperature of 95 ° C, a stirring rate of 250 rpm for a duration of 4 h and a pH 8. In this paper, we refer to this last batch sample as 'DSP-PE-NPs'. The second batch of PE-NP samples was synthesized using an anionic APS initiator in absence of surfactants in order to produce similar PE-NPs in size and chemical nature, but above all without surfactants and with a pristine surface. For the synthesis, the APS and $NaHCO_3$ concentrations were set at 1 $g.L^{-1}$, the ethylene pressure at 100 bar and a temperature of 75 ° C. The stirring rate used was 250 rpm during 4 h at pH 7.8. This batch sample is named 'Bare-PE-NPs'. Following this synthesis protocols, the PE-NPs batches have similar sizes, crystallinities (≈20% from DSC experiments, see Ref. [8]) and the same measured zeta potential at $\zeta \approx$ -40 mV in Milli-Q water.

2.3. Preparation of BSA

The first step to prepare BSA batch solution was to disperse the freezed protein powder in pure Milli-Q water through a long dialysis process (at least 2 h), maintaining a constant temperature of 4 ° C. Subsequently, the solution of BSA underwent two distinct dialysis sessions in 10 mM phosphate buffer (PB) pH 7.2 (for 2 h and 1 h with 5 mL versus 2 L volumes) at same temperature. To eliminate possible BSA aggregates and denatured proteins, an additional centrifugation step was performed at ≈18 300 g (13 200 rpm) for 1 h. The final BSA batch concentration was measured using a NanoDrop 2000 device, which measures the UV–Vis absorption of the solution at the peak absorption wavelength of the BSA λ=278 nm using an external calibration protocol.

2.4. Multi-angle light scattering (MALS)

The size distribution of PE-NP solutions was characterized using dynamic light scattering at several scattering angles (multi-angle light scattering, MALS) in pure water with a ALV-5004 correlator mounted on a ALV-CGS3 goniometer, at 632 nm, before dialysis, at several concentrations and at 20 ° C. MALS data were analyzed using a home-made python program using a unified size distribution model based on log-normal distribution functions fitting simultaneously all auto-correlation curves collected at angles ranging from 14 to 150° with a single distribution curve (more details are given in Appendix C).

2.5. Small angle x-ray scattering (SAXS)

Pure PE-NPs or proteins solutions, as well as their equilibrated mixtures were studied using small angle X-ray scattering experiments at the SOLEIL synchrotron facility at the SWING beamline in the so-called 'BioSAXS' and 'ChemSAXS' configurations [22]. An X-ray wavelength of λ=1.033 Å (12.00 keV) was set for all experiments. The q-range for all experiments was between 0.0011 Å and 0.3 Å. The SAXS data treatment included normalizations with the scattering intensity of pure water and buffer reference solutions were always measured prior to the samples, in order to subtract the scattering contributions arising from various sources, such as the solvent molecules, the air, the quartz capillary walls (2 × 10 μm) and instrument windows (scattering also present while measuring the primary beam without any sample). The pure water scattering corresponds to its known isothermal compressibility, and was used to calibrate the 1D-data in absolute scale of X-ray intensity [cm^{-1}] after radial averaging of the 2D-detector images that shown isotropic scattering for all samples.

Considering a diluted quasi-monodisperse nanoparticles solution, the SAXS intensity can be expressed as follows:

$$I(q) = \int_0^\infty n_p p_z(R) P(q,R) S(q,R) \mathrm{d}R \tag{1}$$

with n_p the density [cm^{-3}] of particles in solution which equals to $\Phi_{v,p} V_p$, $\Phi_{v,p}$ being the volume fraction [no unit], V_p the nanoparticles volume [cm^3] and $\Delta(\rho b)$ the scattering length density contrast which corresponds to the difference between the scattering length densities ρb [cm^{-2}] of the particle material and the solvent (note that ρ_b is equal to the electron density times the scattering length of an electron r_0 = 2.82×10^{-13} cm). $P(q)$ is the particle form factor [cm^2] corresponding to a single particle scattering and $S(q)$ the structure factor [no unit] related to the position correlation function between particles in solution that generate scattering interference contributions to the SAXS signal. $p_z(R)$ represents the z-average radius distribution function (*i.e.* including the fact that larger particles scatter much more than smaller particles at small scattering angles).

All models used to fit the SAXS data are extensively presented in the Appendix A, so we briefly recall here their aims and assumptions: regarding the form factor, PE-NPs were analyzed employing a classical spherical form factor perfectly well adapted to the NPs synthesized, while for BSA proteins, a spheroid form factor following Guinier's description [23] was adopted, as it was demonstrated to perfectly fit the data in many studies [24,25]. Parameters of both models are summarized in left boxes of Fig. 1. For the sphere form factor, the parameters are: $\mu_{R,z}$ and $\sigma_{R,z}$, the average radius and standard deviation of the log-normal distribution, $\Phi_{v,PE}$ the volume fraction (or concentration), ρb_{PE} and ρb_{solv} the scattering length densities of the PE and the solvent. For the spheroid form factor of the BSA, the parameters are: r_p and r_e the polar and equatorial semi-axis, respectively, $\Phi_{v,BSA}$ the volume fraction and ρb_{BSA} and ρb_{solv} the scattering length densities of the BSA and the solvent. In all cases, we used the hard sphere structure factor described by Percus–Yevick closure relation. All experiments were conducted in diluted condition, we did not notice any influence of the structure factor. For the PE-NPs, we added the Teubner-Strey model to adjust the broad correlation peak, I_{TS}, around 0.05 cm^{-1}. This peak is explained by two coexisting phases within PE-NPs particles: crystalline and amorphous phases, which noticeable electronic density fluctuations generating scattering. The crystalline phase is not necessarily a unique homogeneous phase but is more likely multiple crystallized chain domains embedded within the amorphous phase. In our case, we used this model as an empirical approach instead of a real molecular description of the crystal structure, as did in a previous study [21], in order to fit perfectly the PE-NPs SAXS scattering. The parameters of the Teubner-Strey model are: ξ and D^* a total correlation length and domain size, respectively, and η_{TS} a parameter that scales with the volume fraction (see in the appendix for more details).

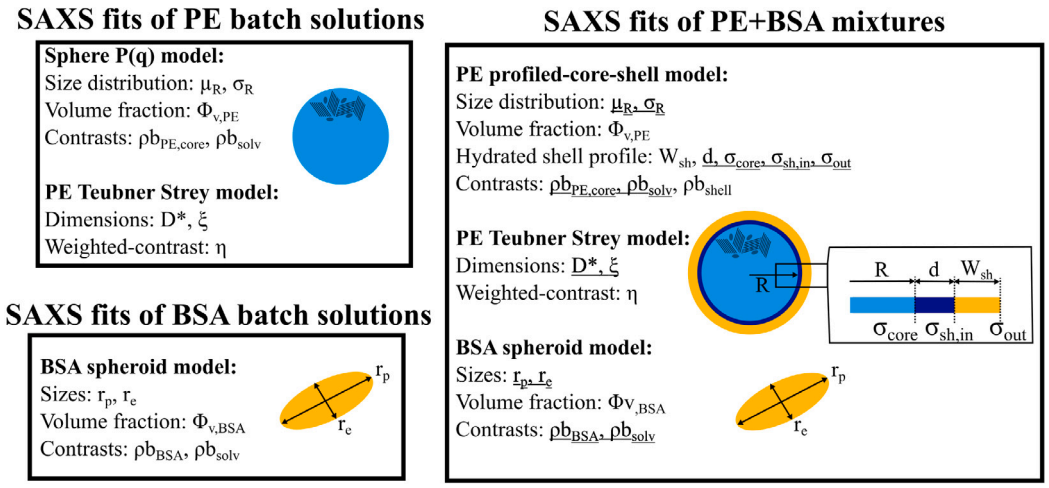

Fig. 1. Workflow of the SAXS data fitting procedure. First, SAXS data from pure PE and BSA batch solutions are fitted to obtain stable structural parameters. These parameters are then fixed for conducting the mixtures fits and are underlined in the figure. Parameters and models are introduced in Appendix A.

With addition of a BSA corona with PE-NPs in solution, we used the profiled-core–shell model. This model adds a concentric shell on the PE surface, featuring a solvent profile with three interface contributions (core/solvent, solvent/shell, shell/solvent) [26–28]. This model gave an excellent fit quality of the SAXS data featuring several oscillations allowing us to reach a spatial resolution going beyond the simple model of a homogeneous shell (classical box-core–shell model). It also accounted for the presence of water molecules near the PE-NP interface within the BSA proteins corona. The profiled-core–shell model includes the following parameters: all parameters of the spherical model, d the water layer thickness between the NPs and the shell, W_{sh} the shell thickness, σ_{core}, $\sigma_{sh,in}$ and σ_{out} the roughness of the core/solvent, solvent/shell, shell/solvent interfaces, respectively. These parameters are summarized in right box of Fig. 1, underlined parameters correspond to the ones fixed at the fitted values of batch solutions.

Data analysis was conducted using SASfit software along with home-made programs. Further details on these models can be found in Appendix A and in Appendix B for more SAXS fitting procedure details.

2.6. Isotherm model

In order to quantify the adsorption of proteins onto colloidal surfaces, we used the Langmuir isotherm model [29] that quantifies protein adsorption (mass per surface unit, denoted as m_{ads} [g.m^{-2}]) as a function of the equilibrium mass concentration of proteins remaining in solution $C_{BSA,free}$ [g.m^{-3}]. This equation depends on two independent parameters: the maximum monolayer adsorption capacity (mass of proteins when the monolayer reaches the saturation of the surface), m_∞ [g.m^{-2}] and the Langmuir adsorption thermodynamical constant K_{ads} [L.g^{-1}], as expressed in the following formula:

$$m_{ads} = \frac{m_\infty K_{ads} C_{BSA,free}}{1 + K_{ads} C_{BSA,free}} \tag{2}$$

This commonly used simple model accurately quantified the adsorbed protein mass we measured while increasing the protein concentration. Evolution of the available surface for adsorption remains a complex task, as discussed in Ref. [12].

To calculate the mass of adsorbed BSA m_{ads} from SAXS fits, we estimate the void fraction of BSA within the shell φ_{BSA} from the fitted scattering length densities of the shell ρb_{shell}, only composed of hydrated BSA proteins ρb_{BSA} and included solvent molecules ρb_{solv}, using the formula:

$$\varphi_{BSA} = \frac{\rho b_{shell} - \rho b_{solv}}{\rho b_{BSA} - \rho b_{solv}} \tag{3}$$

The mean number of BSA proteins adsorbed per particle is then deduced from φ_{BSA} and the maximum number of BSA that can adsorb within the shell:

$$N_{BSA,ads} = \varphi_{BSA} N_{BSA,max} = \varphi_{BSA} \frac{V_{shell}}{V_{1BSA}} \tag{4}$$

Consequently, the corresponding mass of adsorbed BSA is: $m_{BSA_{ads}} = N_{BSA,ads} m_{1BSA}$. To relate this mass to the surface of the particles, we need to know the n-average of the total plastic surface in solution. Since we used a log-normal distribution of the NPs radius to fit the form factor from the data, we established the z-distribution in size $\tilde{p}_z(R)$ from two fit parameters $\mu_{R,z}$ and $\sigma_{R,z}$. By transforming $\tilde{p}_z(R)$ in a n-average surface distribution $\tilde{p}_n(S)$ we obtain:

$$m_{ads}[\text{mg.m}^{-2}] = \frac{m_{BSA_{ads}}}{\int_0^\infty S\tilde{p}_n(S)\text{d}S}$$

$$m_{ads}[\text{mg.m}^{-2}] = \frac{V_{shell}}{V_{1BSA}} \left(\frac{\rho b_{shell} - \rho b_{H_2O}}{\rho b_{BSA} - \rho b_{H_2O}} \right) \times m_{1BSA} \exp\left(-2\mu_{R,z} + 12\sigma_{R,z}^2 - \ln(4\pi)\right) \tag{5}$$

3. Results and discussion

3.1. Pure PE-NP and pure BSA batch solutions

The SAXS data of pure PE-NPs in solution and the corresponding best fits to the SAXS data are plotted in Figs. 2. In Fig. 2-A), we present SAXS intensity curves, for DSP nanoparticles at 0.5%w/w (weight of PE-NPs per weight of the solution) and at several concentrations after filtration through a 0.45 μm filter in pure water. DSP is a disponil (≈1500 g.mol^{-1}) amphiphilic molecule with an C_{12} hydrophobic alkyl chain graft to a PEO_{30} hydrophilic pegylated chain used to stabilized the NPs during their synthesis. The Fig. 2-B) corresponds to SAXS intensities of Bare-PE-NPs (without surfactants) built for two concentrations without filtration in pure water. For those fits, we used a spherical form factor and data were fitted using a homemade program that fit all data at once with common parameters (such as radii or scattering length densities), to get an average value of fitted parameters for all measurements. Also, since the particles Teubner-Strey peak scales with the NPs concentration, we linked its amplitude variation with the NPs dilution factor obtained from the fits of the PE-NPs volume fraction.

The intensity at low q increases with the PE-NPs concentration, as expected for both PE-NPs batches. We found that after filtration, ≈4% of the particles volume fraction decreases slightly (Φ_v=3.02 × 10^{-3} → 2.90×10^{-3}). The fitted scattering length density of DSP-PE-NPs particles

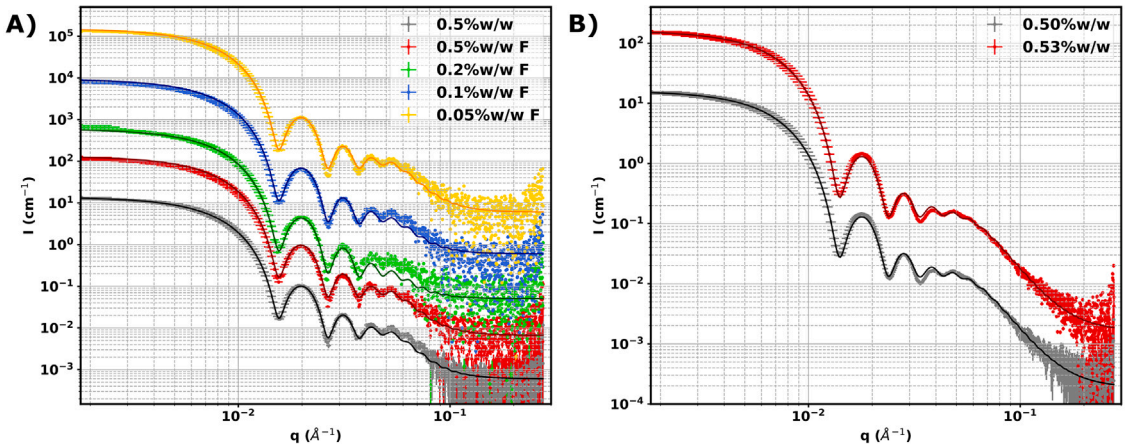

Fig. 2. (A) SAXS intensity curves after background subtraction for the batch DSP-PE-NPs solutions in water at several concentrations. The letter F in the legend denotes samples filtrated at 0.45 μm. Full lines correspond to the best fits to the data (model described in appendix); (B) SAXS intensity curves for the batch Bare-PE-NPs solutions in water; Gray curves are plotted in absolute scale of the intensity [cm^{-1}] and a multiplier is applied to the other curves for readability (×10 red, $\times 10^2$ green, $\times 10^3$ blue, $\times 10^4$ yellow).

is $\langle \rho b_{PE} \rangle$=8.720 × 10^{-6} $Å^{-2}$, corresponding to a contrast with water of $\Delta(\rho b_{PE,w})$=0.653 × 10^{-6} $Å^{-2}$. This value suggests that particles are composed by roughly 68% of amorphous PE and 32% of crystalline PE, which is consistent with the amplitude of correlation peak. The scattering curves exhibit well-defined oscillations yielding an average radius of $\langle R_{mean,PE} \rangle$=29.2 nm, which closely match the values obtained from the MALS fits of the same samples measured between 0.001 and 0.1%w/w (29.3 nm, data shown in the appendix). The standard deviation (σ) of the radius distribution function is smaller from SAXS fits (0.02) than it is from MALS fits (0.25). This difference is probably due the fact that σ is mostly determined by the fit of the form factor oscillations in SAXS experiments and here their amplitudes are damped by the correlation peak corresponding to the PE crystallites (I_{TS}). Therefore, in this particular case, the accuracy expected from SAXS fits is somehow lost for σ determination. All things considered, the NPs solutions can be considered as quasi-monodisperse spheres.

For Bare-PE-NPs, we found a scattering length density of $\langle \rho b_{PE} \rangle$= 8.976 × 10^{-6} $Å^{-2}$, suggesting a slightly higher PE crystallinity than for the DSP-PE-NPs batch. The average size is very similar to the other batch sample as it has been found at $\langle R_{mean,PE} \rangle$=32.3 nm and the polydispersity is low as well (σ_{PE}=0.01).

Since these experiments were carried out during two separate synchrotron beamtimes, we used two BSA batch solutions prepared under the same conditions. The SAXS curves of BSA batch solutions are shown in Fig. 3, both prepared at a concentration of 0.37%w/w in phosphate buffer (PB) 10 mM solvent. As outlined in Appendix A, we employed a spheroid (*i.e.* ellipsoid) form factor for the BSA. For the BSA used in DSP-PE-NPs experiments, the fit corresponds to a polar semi-axis of r_p=18.9 Å and an equatorial semi-axis of r_e=44.4 Å. For the other BSA batch solution, we found similar results with r_p=19.2 Å and r_e=43.6 Å. Therefore, the BSA proteins structure is in a monomeric oblate ellipsoidal form ($r_p < r_e$), as anticipated from this preparation route [24,25]. The fitted BSA volume fractions $\Phi_{v,BSA}$ are 1.56 × 10^{-3} for BSA_{DSP-PE} and 1.94 × 10^{-3} for $BSA_{Bare-PE}$, which are slightly lower than target values due to the protein loss from interactions between BSA with the laboratory vials [30]. Furthermore, the fitted scattering length density ρb_{BSA} matched precisely the expected values from the literature 12.232 × 10^{-6} $Å^{-2}$ for BSA_{DSP-PE} and 12.599 × 10^{-6} $Å^{-2}$ for $BSA_{Bare-PE}$ [24,31,32].

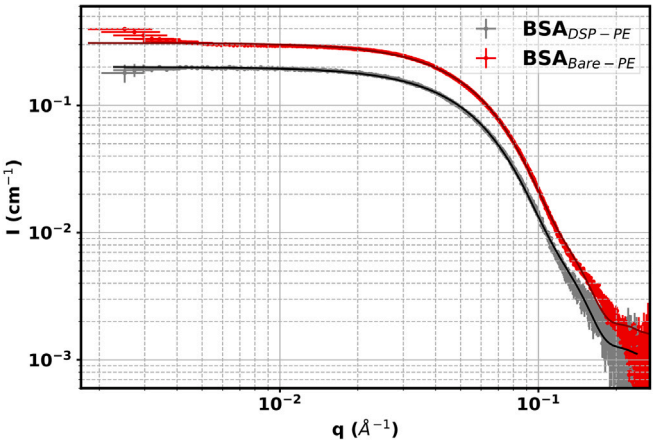

Fig. 3. SAXS intensity curves of the BSA protein solution in PB buffer at 10 mM, pH 7.2 batches used to be exposed to DSP-PE-NPs (BSA_{DSP-PE} in gray) and to Bare-PE-NPs ($BSA_{Bare-PE}$ in red). Best fits to the data are plotted in full lines.

3.2. PE-NP and BSA interactions

To study the interaction of BSA with PE nanoparticles, we conducted two different mixing experiments from the batch solutions described above. In the first procedure, we used DSP-PE-NPs and protein solutions added within the same dialysis membrane bag of 1 mL with a cut off at 3.5 kDa, immersed in a 2 L PB 10 mM reservoir at 20 ° C. The contact time was set to 1 h, for concentrations set to 0.5%w/w for nanoparticles and 1.05 $mg.mL^{-1}$ for BSA. In the second experiment, nanoparticles underwent dialysis in PB 10 mM solution and then mixed to BSA at varying volume ratios X (V_{BSA}/V_{PE-NP}) in sealed vials. In this case, the exposition duration used was always exceeding 30 min, time which proved to be quite sufficient to ensure that equilibrium was reached (rapid Brownian diffusion of BSA and NPs in the mixture). In this way, two mixing protocols will be compared in terms of protein corona formation for the DSP-PE-NPs. The first experiment was conducted to test the removal of DSP surfactants *via* dialysis while simultaneously adsorbing BSA on the DSP-PE-NPs, in order to maintain colloidal stability. This experience also enabled us to choose the SAXS models to consider for the second experiment, where we mixed dialyzed NPs with BSA to draw the isotherms.

3.2.1. Protocol 1: Interactions between DSP-PE-NPs and BSA during dialysis against a PB buffer

Two rounds of dialysis (5 mL versus 2 L) were carried out, each lasting for 1 h in PB 10 mM at 20 ° C, to eliminate residual traces

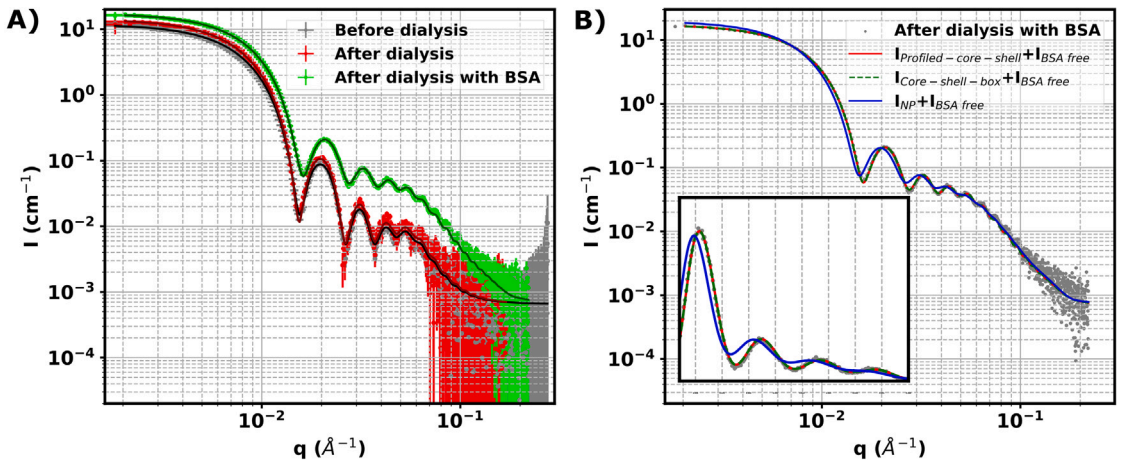

Fig. 4. (A) SAXS intensity curves of DSP-PE-NPs measured before dialysis (PE 0.5%w/w F, in gray), after dialysis (in red) and then dialyzed with addition of BSA protein in PB 10 mM, pH 7.2 (in green). (B) three models used to fit the SAXS curves of DSP-PE-NPs dialyzed with BSA (explained in the text). The inset is a zoom of the first oscillations.

of neutral surfactants (DSP) used to stabilized DSP-PE-NPs. As shown in Fig. 4-A), the SAXS intensity curve of PE-NPs is unchanged upon dialysis in PB buffer (gray to red curve), meaning that the stability is kept and that no aggregation occurs. The particles remain stable probably due to remaining DSP surfactants bounded *via* strong hydrophobic interactions or co-crystallization of their alkyl chains with PE. Stability also arises from electrostatic repulsion from surface charges existing on the NPs ($\zeta \approx$ -40 mV in water). Such charges are expected from: OH- ions that tends to adsorb onto hydrophobic surfaces or secondary reactions from the initiator degradation during the polymerization creating COO- charges. Note that the contrast between possibly bound DSP PEG chains (-H(OCH_2CH_2)$_{30}$OH) and the solvent is too small to be detected here (the scattering length density of PEG_{30} is estimated around ρb_{PEG30}=9.2 to 9.3 × 10^{-6} Å^{-2} [33], and once highly hydrated in water it is indistinguishable from water (ρb_{water}=9.373 × 10^{-6} Å^{-2}). The SAXS curve of the BSA/PE-NPs mixture after dialysis corresponds to the green curve, revealing two key changes: 1) a significant increase of the absolute scale intensity arising from the added free BSA proteins in solution (*via* their form factor) and 2) a slight shift of the particles oscillations towards higher values of q.

To model the scattering curve of PE-NPs and BSA mixture at equilibrium, we considered three hypothetical models:

- Model 1 (shown in blue in Fig. 4-B)): Assumes an absence of interaction between BSA and PE-NPs. The intensity is then calculated from the sum of their individual contributions: $I(q) = I_{PE\text{-}NPs}(q) + I_{BSA}(q)$. Specifically, it combines the functions previously described for both components (NPs: spherical form factor $P(q)$, hard sphere Percus–Yevick structure factor $S(q)$, integrated over a log-normal size distribution and the Teubner-Strey model for the correlation peak $I_{TS}(q)$; BSA: spheroid form factor $P(q)$ and hard sphere structure factor $S(q)$). We neglected here scattering cross terms expected from coherent interferences between scattered signals arising from NPs and free BSA (as expected at high dilutions).
- Model 2 (shown in green in Fig. 4-B)): Posits that BSA proteins interact with PE-NPs, forming a uniform BSA shell (corona with a water content as well). In this model we used: $I_{NP}(q)$ the classical box core–shell form factor $P(q)$, the hard sphere Percus–Yevick structure factor $S(q)$, both integrated over a log-normal radius distribution and the Teubner-Strey model $I_{TS}(q)$; Other BSA proteins remain free and hydrated in solution (spheroid $P(q)$ and hard sphere $S(q)$ contributions).
- Model 3 (shown in red in Fig. 4-B)): Integrates a more sophisticated shell model for the NPs (profiled-core–shell form factor), given the presence of solvent molecules in the shell at contact of adsorbed BSA proteins. The rest of the contributions to the total SAXS intensity are described in model 2, here the only change is in the particles $P(q)$.

The best fits of these three models are shown in Fig. 4-B). As no interaction is assumed in the first model, we kept the size distribution constant. Clearly, the first model fails to fit the data accurately, even while fitting again the particles radii, all oscillations are not captured in phases. The second and third models fit quite well to the data with no noticeable difference to the eye. However, the third model results in a lower χ^2 than the second one and this difference increases for samples with more BSA added to the PE-NPs solution. Therefore, the profiled-core–shell model is used to adjust the data when PE-NPs are exposed to BSA. This model can also be justified by the fact that the hydrated BSA proteins bound to the PE-NPs, come with an ellipsoid shape, and result in a rich water content even at the PE surface contact. The best fits to the data results in the following parameters:

- For the PE-NPs:
  $\Phi_{v,PE}$=5.15 × 10^{-3}, R_{mean}=291.5 Å, $\sigma_{log\text{-}norm}$=0.023, σ_{core}=1 Å (interface with the solvent), ρb_{PE}=8.720 × 10^{-6} Å^{-2}.
- For the BSA Corona:
  - Rich solvent layer on PE: D=1 Å (thickness), $\sigma_{sh,in}$=1 Å (roughness with the shell), ρb_{solv}=9.373 × 10^{-6} Å^{-2}.
  - BSA shell: W_{shell}=21.9 Å (thickness), σ_{out}=1 Å (roughness with the solvent), ρb_{shell}=9.743 × 10^{-6} Å^{-2}.
- For the BSA proteins remaining free in solution:
  $\Phi_{v,BSA}$=0.34 × 10^{-3}, r_p=19.0 Å, r_e=44.4 Å, ρb_{BSA}=12.232 × 10^{-6} Å^{-2}.

The parameters pertaining to the PE core and to the unadsorbed free BSA in solution were fitted first and then fixed to the values obtained from pure batch solutions without affecting the quality of the fit and the determination of other parameters. Using these parameters, the scattering length density profile $\rho b(r)$ has been computed as well as the void fraction φ of each component (see Appendix A). Upon examining the BSA fraction profile, we determined about 12.94% of BSA proteins within the corona (corresponding to roughly 24 BSA per NPs), resulting in a total mass of adsorbed BSA m_{ads}=0.25 mg.m^{-2}. Initially, the BSA concentration stood at 1.05 mg.mL^{-1}, but it had dropped down to 0.45 mg.mL^{-1} due to the expected dilution resulting from the mixing with PE-NP solution in the dialysis bag, adsorption and protein losses

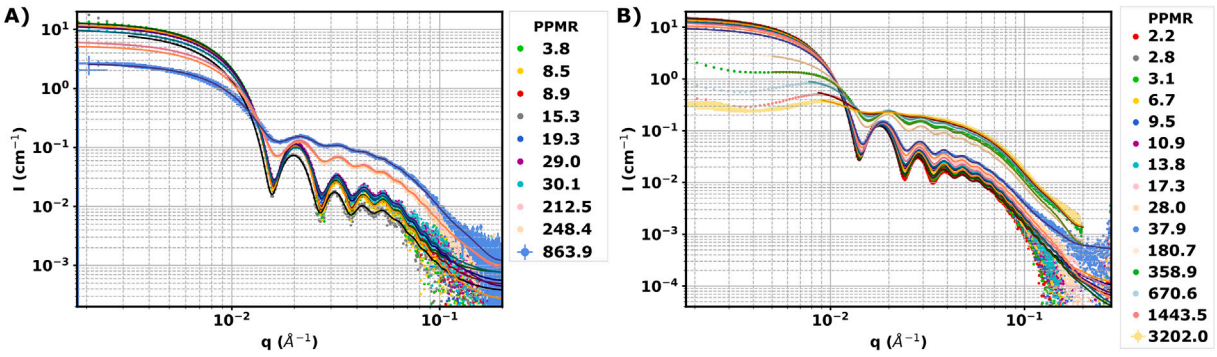

Fig. 5. SAXS curves from mixtures of DSP-PE-NPs/BSA proteins (Figure A)) and Bare-PE-NPs/BSA (Figure B)) in PB 10 mM, pH 7.2 at several PPMR (or mixing ratio X). Best fits to the data are plotted on top with full lines and darkest color set.

attributed to interactions with vials and laboratory consumables [30] can also participate to this.

During the dialysis against the buffer, the corona formed well on particles synthesized with DSP surfactants (DSP-PE-NPs), even if we could not exclude remaining traces of DSP at the NPs surfaces. Since we may have not reached here the surface saturation value, we built the following protocol to study the adsorption isotherms.

3.2.2. Protocol 2: Interactions between PE-NPs and BSA mixed at different molar ratio

In order to gain a deeper understanding of BSA corona formation on the surfaces of dialyzed PE nanoparticles, we prepared mixtures of BSA and PE at several volume ratios X ($X = V_{Prot}/V_{NP}$) in PB 10 mM, pH 7.2, at fixed mixture volume and keeping the mass concentration of the total mixture constant at 0.37%w/w for DSP-PE-NPs mixtures and 0.5%w/w for Bare-PE-NPs. The ratio X also corresponds to the mass concentration ratio of BSA by PE-NPs. This ratio is converted to Protein-to-Particle Molar Ratio (PPMR) by the following formula: $\text{PPMR} = X M_{w,NP}/M_{w,BSA}$, where $M_{w,NP}$ and $M_{w,BSA}$ are the molecular weights of nanoparticles and proteins, respectively. Fig. 5 presents the scattering intensity of the different samples, with PPMR varying from 4 to 864 for DSP-PE-NPs and from 2 to 3202 for Bare-PE-NPs (corresponding approximately to X from 7×10^{-3} to 1.6 and 4×10^{-3} to 6, respectively). At small PPMR values, PE-NPs concentration significantly outweighs the BSA concentration within the mixture. Thus, the SAXS data is similar to the one measured on PE-NPs batch solutions with a clear intensity plateau at low q values that scales with their concentration (so-called the Guinier plateau for the PE-NPs form factor). When PPMR increases, the PE-NPs form factor oscillations that come after the plateau become progressively less pronounced since they are damped by a noticeable additional intensity contribution coming from the scattering of free BSA proteins in solution (see beyond 0.01 $Å^{-1}$). It is also important to note that the oscillations progressively shift towards higher q values while the relative amount of BSA increases for the sample.

As before, we used the profiled-core–shell form factor model to fit the SAXS data including the BSA corona formation. The choices and key elements that led to excellent fits are now discussed (see the Appendix B for the detailed procedure). The fitted parameters that change between samples are: $\Phi_{v,PE}$, $\Phi_{v,BSA,free}$, the PE-NPs and BSA volume fractions, respectively, W_{shell} the shell (corona) thickness, ρb_{shell} the shell scattering length density, η_{TS} the parameter controlling the Teubner-Strey intensity and a constant background scattering. Note that for the BSA concentrations used, the scattering length density of the solvent involved in this form factor calculation, does not evolve significantly with X. In addition, the Teubner-Strey scattering contribution from PE crystallites evolves linearly with the PE-NP volume fraction.

The shift of the NP form factor oscillations is related to a change in size or to a change in contrast of the PE-NPs form factor due to BSA addition in the shell. Thus, the thickness W_{shell} and the scattering length density of the shell ρb_{shell}, may vary simultaneously and are correlated parameters. For this reason, we deduced the number of BSA adsorbed per PE-NP combining simultaneously the effect of both parameters evolution (*i.e.* if W_{shell} decreases, ρb_{shell} increases and vice versa). For DSP-PE-NPs samples, we found a change in ρb_{shell} from 9.48×10^{-6} $Å^{-2}$ to 9.85×10^{-6} $Å^{-2}$ and a shell thickness evolving from 1.0 Å to 30.8 Å. This leads to a number of BSA per particle's corona that increases from 2 to 43 proteins (for PPMR between 15.3 and 863.9, respectively). In the case of Bare-PE-NPs samples, ρb_{shell} varies from 9.38×10^{-6} $Å^{-2}$ to 9.78×10^{-6} $Å^{-2}$ while W_{shell} increases from 24.6 Å to 65.9 Å for PPMR ranging from 2.2 to 3202, corresponding to 1 to 75 BSA per corona, respectively. All fitted parameters are shown in the appendix Tables E.1 and E.3. To get the isotherm, we used the intermediate variables shown in 2.6 that are shown in the appendix Tables E.2 and E.4. Using Eq. (5) we deduce the mass of adsorbed BSA per surface unit of PE-NPs that rises to 0.45 $mg.m^2$ for DSP-PE-NPs and 0.64 $mg.m^{-2}$ for Bare-PE-NPs.

To simultaneously determine the amount of unadsorbed BSA mass, we fitted $\Phi_{v,BSA}$ that scales with the scattering contribution from the BSA ellipsoid form factor. In the DSP-PE-NPs experiment, it corresponds to free BSA concentrations ranging from 0.06 to 1.66 $mg.mL^{-1}$, while in the Bare-PE-NPs experiment to concentrations from 0.02 to 1.97 $mg.mL^{-1}$. The PE-NPs with a BSA corona formed at equilibrium with free proteins in solution, are well stabilized in solution (in 10 mM PB) and the scattering curves do not show particles aggregation. Except in one case, for the DSP-PE-NPs sample equilibrated with the smallest amount of BSA tested (*i.e.* smallest PPMR). In this case, we observed a noticeable increase of the SAXS intensity at small q values instead of a Guinier plateau, that is due to bridging of PE-NP particles by BSA proteins (Fig. 5-A).

From the fits we built the adsorption isotherms of the BSA on DSP-PE-NPs and Bare-PE-NPs surfaces (shown in Fig. 6). Good fits of both isotherms were achieved using the Langmuir model (Eq. (2), red lines plotted on top of the data). The point measured from the first DSP-PE-NPs experiment is also plotted in gray for comparison.

The Langmuir isotherm model describes our data very well, and from the fits we deduce a maximum monolayer adsorption capacity (expressed in the form of a saturation mass of BSA per meter square of PE interface, once a single monolayer of proteins forms the corona), m_∞. We obtained m_∞=0.50 ± 0.05 $mg.m^{-2}$ for DSP-PE-NPs samples and m_∞=1.51 ± 0.26 $mg.m^{-2}$ for Bare-PE-NPs samples. The fits also quantify an adsorption Langmuir constant of K_{ads}=3.15 ± 0.91 $L.g^{-1}$ for DSP-PE-NPs, and 0.41 ± 0.11 $L.g^{-1}$ for Bare-PE-NPs. Different values are due to the differences in NPs surface chemistry. Concerning the adsorbed BSA mass at the saturation plateau m_∞, we find more adsorbed BSA at saturation for the Bare-PE-NPs. This probably comes from the fact that DSP-PE-NPs have an additional steric hindrance from PEG chains of remaining DSP molecules. However, we observe a stronger affinity for BSA adsorption by DSP-PE-NPs (quantified *via* K_{ads}), suggesting that residual DSP surfactants at PE-NP surfaces, favor the BSA

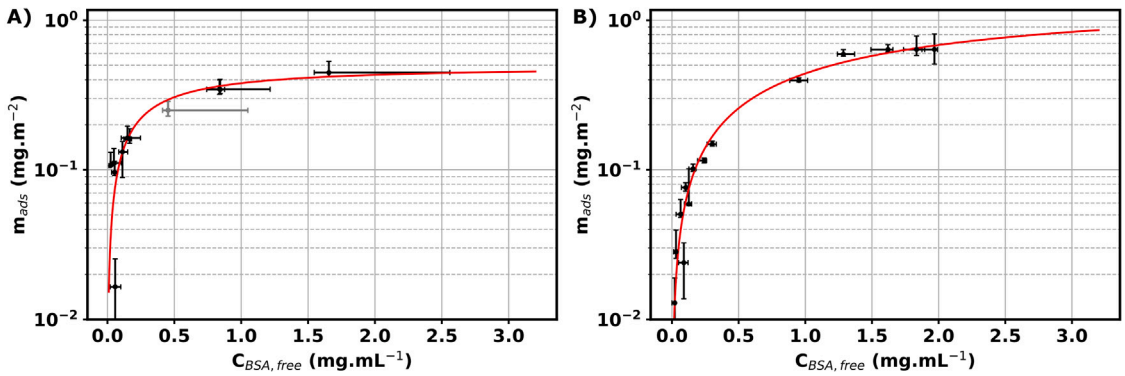

Fig. 6. Adsorption isotherms of BSA on **(A)** DSP-PE-NPs and **(B)** Bare-PE-NPs in PB 10 mM, pH 7.2 obtained from SAXS best fit parameters. Experimental data are black dots with confidence intervals along x and y axis (see Appendix B.3) and the fitted Langmuir models correspond the red full lines. The gray dot on the left plot represents the result from the first experiment.

adsorption. PEG chains are known protein antifouling agents [34] but their amount here was significantly reduced by extensive dialysis so that BSA adsorption remains favorable. Another explanation would be that the COO- or OH- at the surface of the DSP-PE-NPs promote more stabilizing interactions with BSA, such as hydrogen bonding, than the SO_3^- of the Bare-PE-NPs surface.

Our BSA isotherms compare also very well with those published for the interaction with commercial 40 nm silica NPs (Aerosil OX-50 Degussa, at 42 m^2.g^{-1} and zeta potential $\zeta \approx$-48 mV from -O$^-$ groups) and with negatively charged polystyrene nanolatex (diameters larger than 200 nm at 8 m^2.g^{-1} and $\zeta \approx$-69 mV from -SO_3^- groups) obtained under similar solvent conditions (10 mM phosphate buffer at pH 7) so well above the BSA isoelectric point (pH 4.7) [35]. From these data (Fig. 1 [35]), we fitted Langmuir isotherms corresponding to the following constants: K_{ads}=8.22 ± 1.13 L.g^{-1} and m_∞=1.01 ± 0.04 mg.m^{-2} for silica NPs, or K_{ads}=7.58 ± 2.66 L.g^{-1} and m_∞=1.03 ± 0.05 mg.m^{-2} for polystyrene NPs. Indicating a slightly higher BSA/NP affinity for SiO_2 and PS than for PE-NPs but a similar saturation mass. Here, BSA adsorb on PE nanoparticles even under unfavorable electrostatic global interactions (proteins and sorbent surfaces have similar negative zeta potentials). Attractive interactions are thus sufficiently strong and involve: dispersion forces (such as Van der Waals), local electrostatics between surface and oppositely charged BSA groups, conformational changes of the BSA and water molecules or ions that are displaced from the surface corresponding to a global entropic gain. Such structural rearrangements in the adsorbed BSA shell are expected to play a major role in the adsorption process and explain why it is a favorable process against global electrostatic repulsion. Affinity is expected to increase at pHs canceling net charges (isoelectric points).

We recently measured adsorption isotherms of BSA on pristine PE microplastics (4 μm diameter) using the Bradford and depletion methods [36]. A Langmuir model yielded a saturation surface concentration of $m_\infty = (1.5 \pm 0.1)$ mg· m^{-2} and an adsorption constant $K_{ads} = (5 \pm 1) \times 10^2$ L· g^{-1}. The K_{ads} value for pristine PE-NPs is much lower than that of PE-MPs, evidencing a markedly weaker BSA affinity attributed to differences in surface chemistry: PE-MPs display a higher hydrophobicity (water contact angle = 116 °), whereas emulsion-synthesized PE-NPs possess more hydrophilic surfaces. The local dehydration of the PE surface is a strong entropic driving force for proteins adsorption which explains the higher affinity of BSA for pristine PE-MPs than for PE-NPs. BSA in its native form (pH range 4.5-7) must be considered as a quite flexible globular protein with a high adaptability to surfaces from its tendency to undergo structural rearrangements upon adsorption (a so-called 'Soft protein' in the Norde classification). When the affinity with the sorbent is high and surface coverage is low, BSA structural changes are strong [37] and this further promotes water displacement from the surface and an entropic gain. Although, BSA adsorbs onto both types of surfaces: on hydrophilic ones (PE-NPs, SiO_2) with a moderate affinity, and on more hydrophobic ones (PE-MPs, PS, Teflon) with a higher affinity, but this implies different secondary structure rearrangements. On hydrophilic surfaces and even in presence of global electrostatic repulsions, the adsorption is noticeably promoted by a BSA net conformational entropy increase due to a loss of its ordered secondary structure, as seen from the decrease of its α-helix content measured by circular dichroism spectroscopy [38]. This is accompanied by a gain in peptide units mobility and a reconfiguration of hydrogen bonding (intra and inter molecular). Upon adsorption on quite hydrophobic surfaces (such as PS films or Teflon), an intramolecular development of its β-sheets structure at the expense of a α-helix content was measured corresponding to a more stable state [39].

Adsorbed proteins are expected to desorb from the PE-NPs, either by exchange with free proteins (homo-molecular exchange) or by displacement from other chemicals (surfactants, solvent, ions). In the frame of the Langmuir model this is expected *via* dilution with an affinity constant that is unchanged through subsequent interactions (reversible adsorption). This model hypothesis is supported for BSA proteins since they are known to re-adopt their native three-dimensional structure after desorption from surfaces that compares to our PE-NPs surfaces in terms of hydrophilicity [39]. On the opposite, on highly hydrophobic surfaces, soft proteins that would experience a spread conformation at adsorption would keep persistent structural changes after homo-molecular desorption.

Considering the plateau value of the isotherms measured, we can estimate from a flat surface a maximum adsorbed amount of native form BSA proteins around 4 mg.m^{-2} so respectively that would translate, neglecting curvature effects, in 1.9 mg.m^{-2} proteins on DSP-PE-NP and Bare-PE-NPs. As expected, we measured smaller values given by the fitted m_∞ Langmuir constant. Surprisingly, the fitted m_∞ for NPs compares well with the one determined for MPs, while we anticipated a difference at saturation due to the steric effect that predicts lower values for the highest PE interface curvature [40]. Although, we noticed for Bare-PE-NPs a thickening of the fitted BSA shell from the SAXS analysis, W_{sh} up to 60 Å (with 12% of the volume occupied by BSA this corresponds to 75 BSA molecules per NPs), while for DSP-PE-NPs, W_{sh} reaches 30 Å (with BSA occupying 17% of the volume, so a maximum of 43 BSA molecules per nanoparticle). The Freundlich isotherm, which considers the formation of a multilayer corona, has been also tested on the SAXS data but it did not provide a better fit to the data. Partially grown BSA multilayers might not be excluded (soft outer corona) at higher BSA concentrations, and the dimerization of BSA in solution can appear as well since almost entirely dimeric BSA is expected above 8 mg/mL (conditions not explored in our case).

4. Conclusion

We conducted quantitative SAXS experiments of mixtures from polyethylene individualized nanoparticles (PE-NPs) and native BSA

monomeric proteins, as stated from SAXS fits, to study their interactions and the protein corona formation in 10 mM phosphate buffer solutions. At pH 7.2, that is well above the BSA isoelectric point, both interactants are negatively charged ($\zeta \approx$-40 mV) in biorelevant conditions. Excellent fits to the SAXS data in absolute unit scale [cm^{-1}] over a large q range (10^{-3}-0.3 $Å^{-1}$) were obtained for all mixtures. The analysis model was built to measure simultaneously the number of adsorbed proteins in the nanoparticles shell, the water content (protein corona), as well as the concentration of free proteins remaining in solution at equilibrium. The SAXS data of batch solutions prepared before mixing shows that the synthesized PE-NPs can be considered as model spherical and monodisperse nanoplastics with a controlled PE crystallinity degree. Similarly, the BSA proteins solutions were well stabilized in their monomeric form in the same buffer solution, showing no evolution even after long contact times with the nanoparticles. Then, we first studied the mixture of PE-NPs (around 5 $mg.mL^{-1}$) with BSA proteins (at 1.05 $mg.mL^{-1}$), directly into a dialysis bag upon dialysis over long times and volumes against the pure buffer, leading to a BSA adsorption and corona formation. To go deeper in the understanding of the corona formation, we further performed mixing experiments in sealed vials at different molar and concentration ratios, in order to measure the adsorption isothermal equilibrium states. From the SAXS data we built the adsorption isotherms over a large range of proteins concentration (0.02 to 2 $mg.mL^{-1}$) and interactants molar ratios (X from 4×10^{-3} to 6, *i.e.* PPMR from 2.2 to 3202, respectively). Measured isotherms were well fitted using the thermodynamical Langmuir isotherm model that corresponds to a protein monolayer formation in equilibrium with native proteins in solution. We found that over a large range of conditions, the BSA corona forms on both PE-NPs synthesized, with or without surfactant involved. It also appears that the Bare-PE-NPs (synthesized without surfactants) adsorb slightly more proteins at its surface saturation (high BSA concentration) than the one built with disponil surfactants and dialyzed. This is related to different proteins crowding on the saturated corona. Nevertheless, in both cases, we find a strong interaction of BSA proteins with PE nanoparticles, comparable to what measured previously on silicate and polystyrene nanoparticles. The adsorption involves entropically favorable dehydration of the particle interface, related to remodeling of the BSA conformation, beating the net repulsive electrostatic interaction. The Langmuir isotherms obtained for PE nanoparticles show comparable levels of adsorption at saturation (m_∞) than the ones previously measured from PE microparticles (PE-MPs). On the other hand, the affinity constant (K_{ads}) is two orders of magnitude smaller for PE-NPs than for PE-MPs. The much higher affinity of BSA for PE-MPs than for PE-NPs, results from the higher PE microparticles hydrophobicity, which arises from differences in surface properties (such as charges, hydrophilicities, cristallinities) and differences of their interfacial curvatures. Quantitative SAXS analysis was demonstrated here to be an efficient approach to finely characterize the BSA protein corona formation on polyethylene and to consequently study fundamental parameters related to plastics/proteins interactions. This work also shows that well controlled synthesized NPs (in presence or absence of surfactants), are excellent candidates for building model nanoplastics stabilized in aqueous solutions by proteins. Such model particles are particularly sought for conducting other types of bioassays, such as for ecotoxicological studies related to the fate and interactions of nanoplastics within biotic or abiotic environments.

CRediT authorship contribution statement

Thomas Perrault: Writing – original draft, Visualization, Software, Methodology, Investigation, Formal analysis, Data curation. **Léa Jacquin:** Writing – review & editing, Investigation, Data curation. **Marion Schvartz:** Writing – review & editing, Investigation. **Florent Saudrais:** Investigation. **Aurélien Thureau:** Writing – review & editing, Resources, Data curation. **Vincent Monteil:** Writing – review & editing, Supervision. **Serge Pin:** Writing – review & editing, Supervision. **Yves Boulard:** Writing – review & editing, Supervision, Project administration. **Jean-Philippe Renault:** Writing – review & editing, Supervision, Project administration, Conceptualization. **Fabrice Brunel:** Writing – review & editing, Validation, Project administration, Methodology, Investigation, Funding acquisition, Data curation, Conceptualization. **Guillaume Brotons:** Writing – original draft, Visualization, Validation, Supervision, Software, Project administration, Methodology, Investigation, Funding acquisition, Formal analysis, Data curation, Conceptualization.

Declaration of competing interest

The authors declare that they have no known competing financial interests or personal relationships that could have appeared to influence the work reported in this paper.

Acknowledgments

This work, along with Perrault Th.'s PhD funding, was supported by the French National Research Program for Environmental and Occupational Health of ANSES (2018/1/194 PROMPT). Financial support from the French National Research Agency (ANR) is gratefully acknowledged, in particular for Jacquin L.'s PhD grant (ANR-CE06-0019-01 POEM). Schvartz M. received doctoral funding jointly provided by the Pays de la Loire Region and the CEA, while Saudrais F. benefited from a PhD grant overseen by the CEA. We gratefully thank the Synchrotron SOLEIL for the beamtimes allocated (proposals 20211679 and 20231534) and the SWING beamline team for providing excellent working conditions.

Appendix A. SAXS intensity models

SAXS experiments entail the measurement of the scattered X-ray intensities, as a function of the scattering vector q [$Å^{-1}$], from solutions of nanoparticles, proteins, and their mixtures. The X-ray scattering contrast, between particles and solvent, comes from the effective electron density at 12 keV energy and is expressed in the form of a scattering length density contrast [cm^{-2} or $Å^{-2}$]. The SAXS intensity can be expressed as follows in our case:

$$I(q) = \Phi_{v,p} V_p (\Delta(\rho b))^2 \tilde{P}(q) S(q) = n_p P(q) S(q) \quad \text{(A.1)}$$

with $\Phi_{v,p}$ the volume fraction of particles [no units], V_p the particle volume [cm^3] and n_p the density of particles in solution [cm^{-3}]. $P(q)$ and $\tilde{P}(q)$ are, the form factor [cm^2] and the normalized form factor [no units] ($\tilde{P}(q \to 0) = 1$), respectively, both obtained from the Fourier transform of the 3D electron density distribution. $S(q)$ is the particles structure factor [no units] related to the correlations of particles positions ($S(q) = 1$ at high dilution). $\Delta(\rho b)$ is the scattering length density contrast, obtained from the difference of scattering length densities ρb, between the particles and the solvent. For X-rays, the scattering length density is roughly equal to the electron density ρ_e [cm^{-3}] times the scattering length of an electron r_0=2.8179 $\times$ 10^{-13} cm (the classical electron radius), as:

$$(\rho b) = r_0 \rho_e = r_0 d \mathcal{N}_A \frac{\sum_i \varphi_i (Z_i + f_i')}{\sum_i \varphi_i A_i} \quad \text{(A.2)}$$

where d is the density of the considered material [$g.cm^{-3}$]. The index i denotes the atoms that compose the material, A is the molar mass of its atoms [$g.mol^{-1}$] and $Z + f'$ is the number of effective electrons of the atoms interacting with X-rays (f' is a correction factor that depends on the X-ray energy). φ is a weighting factor related to the total number of the atom i in the considered material. For instance, regarding H_2O: φ_H=2 and φ_O=1, so ρb_{H2O}=9.46 $\times$ $10^{-6} Å^{-2}$ at 12 keV.

When considering a polydisperse particles population, the overall scattered intensity must be integrated over the z-average distribution function of particles. For spherical particles of radius R:

$$I(q) = \int_0^\infty n_p p_z(R) P(q,R) S(q,R) \mathrm{d}R \tag{A.3}$$

We considered a Log-Normal distribution of radii. The main advantage of this distribution is that it is only defined for positive values of its variable ($R \in [0,\infty[$) with a zero probability for $R \to 0$ $\forall$ its function parameters μ and σ. For instance, considering the log-normal distribution written for the radius (normalized by its total surface), we have:

$$\tilde{p}(R,\mu,\sigma) = \frac{1}{R\sigma\sqrt{2\pi}} \exp\left(-\frac{1}{2}\left(\frac{\ln(R)-\mu}{\sigma}\right)\right)^2 \tag{A.4}$$

with parameters: σ, the standard deviation ($\sigma > 0$) which gives the geometric standard deviation $\exp(\sigma)$; μ, the average ($-\infty < \mu < +\infty$) which can be expressed in the form of a geometrical average of the radius $R_{\mathrm{median}} = \exp(\mu)$. All of its n-order momentum are defined analytically:

$$M_{n,R} = \langle R^n \rangle \equiv \int_0^\infty R^n \tilde{p}(R)\mathrm{d}R = \exp\left(n\mu + \frac{n^2}{2}\sigma^2\right) = R_{\mathrm{median}}^n \exp\left(\frac{n^2}{2}\sigma^2\right) \tag{A.5}$$

The first momenta corresponds to the mean of the distribution radius R_{mean}:

$$M_{1,R} = R_{\mathrm{mean}} = \langle R \rangle = \int_0^\infty R\tilde{p}(R)\mathrm{d}R = \exp\left(\mu + \frac{1}{2}\sigma^2\right) = R_{\mathrm{median}} \exp\left(\frac{1}{2}\sigma^2\right) \tag{A.6}$$

The hard sphere structure factor obtained from the Percus–Yevick closure relation for 3D hard spheres [41,42]. It was used to take into account particles interactions and it writes:

$$S(q,R,\Phi_v) = \left(1 + 24\Phi_v \frac{G(\Phi_v,A)}{A}\right)^{-1} \tag{A.7}$$

For a hard sphere interaction potential ($V = \infty$ if $r \le R$ and $V = 0$ if $r < R$). We also have:

$$\alpha = \frac{(1+2\Phi_v)^2}{(1-\Phi_v)^4},\ \beta = -6\Phi_v\frac{(1+\Phi_v/2)^2}{(1-\Phi_v)^4},\ \gamma = \frac{\Phi_v\alpha}{2},\ A = 2Rq \tag{A.8}$$

$$G(\Phi_v,A) = \alpha\frac{\sin A - A\sin A}{A^2} + \beta\frac{2A\sin A + (2-A^2)\cos A - 2}{A^3} + \\ + \gamma\frac{-A^4\cos A + 4[(3A^2-6)\cos A + (A^3-6A)\sin A + 1]}{A^5} \tag{A.9}$$

The scattering function from a bare PE-NPs was modeled by the classical spherical form factor $P(q)$, which writes:

$$P(q) = (\Delta(\rho b))^2 V^2 \left|\frac{3(\sin(qR) - qR\cos(qR))}{(qR)^3}\right|^2 \tag{A.10}$$

As explained in the main manuscript, we added a Teubner-Strey scattering component [43] to describe the scattered intensity due to spatial fluctuations of the internal electron density arising from crystallized domains within amorphous PE nanoparticles. This model is calculated from the following expression [44]:

$$I(q) = \frac{I_0}{a + bq^2 + cq^4} \tag{A.11}$$

This equation depends on two characteristic lengths (obtained from three parameters: a, b and c): D^*, a mean periodicity associated to the characteristic domains sizes and ξ, a total correlation length. It corresponds to the distance over which the scattering length density correlation function decreases by a factor $\exp(-1)$=0.3679, according to the Debye and Bueche model [45,46]:

$$g(r) = \frac{\langle \rho b(0)\rho b(r)\rangle}{\left\langle \left(\rho b(r) - \bar{\rho b}\right)^2\right\rangle} = \exp\left(-\frac{r}{\xi}\right) \tag{A.12}$$

with ρb the scattering length density and $\bar{\rho b}$ the average scattering length density given by: $\bar{\rho b} = \Phi_v \rho b_A + (1-\Phi_v)\rho b_B$ where Φ_v and $(1-\Phi_v)$ are the volume fractions of the phases A and B (here crystalline and amorphous PE), respectively. From Eq. (A.11), the correlation length is given by:

$$\xi = \left(\frac{1}{2}\sqrt{\frac{a}{c}} + \frac{1}{4}\sqrt{\frac{b}{c}}\right)^{-\frac{1}{2}} \tag{A.13}$$

And the domain size D^* by:

$$D^* = 2\pi\left(\frac{1}{2}\sqrt{\frac{a}{c}} - \frac{1}{4}\sqrt{\frac{b}{c}}\right)^{-\frac{1}{2}} \tag{A.14}$$

The forward intensity I_0 [cm^{-1}], corresponding to $I(q)$ at $q \to 0$ such as $I(q \to 0) = I_0/a$, writes:

$$I_0 = \frac{2\pi c.4\left\langle \Phi_v(1-\Phi_v)(\Delta(\rho b))^2\right\rangle}{\xi} \tag{A.15}$$

with $\Delta(\rho b)$ the contrast between the scattering length densities of A and B regions ($\Delta(\rho b) = \rho b_A - \rho b_B$). We used another form of Eq. (A.11) which writes:

$$I(q) = \frac{I_0}{1 + q_m^2 q^2 + cq^4} \tag{A.16}$$

Thus we find:

$$I_0 = \frac{2\pi D^{*4} 4\left\langle \Phi_v(1-\Phi_v)(\Delta(\rho b))^2\right\rangle \xi^3}{\left(D^{*2} + 4\pi^2\xi^2\right)^2},\ q_m^2 = \frac{2D^{*2}\xi^2(D^{*2} - 4\pi^2\xi^2)}{\left(D^{*2} + 4\pi^2\xi^2\right)^2},\\ c = \frac{D^{*4}\xi^4}{\left(D^{*2} + 4\pi^2\xi^2\right)^2} \tag{A.17}$$

Practically, it is even possible to quantity the void fractions of crystalline and amorphous phases in the PE nanoparticles (i_c and i_a in %) knowing their respective scattering length densities and their total volume fractions since: $\left\langle \Phi_v(1-\Phi_v)(\Delta(\rho b))^2\right\rangle = \left\langle i_a i_c(\Delta(\rho b))^2\right\rangle / \Phi_v^2$. Fig. A.7 shows the best fit (black line) to a SAXS 1D-data curve measured from a DSP-PE-NPs sample (PE nanoparticles batch sample at 0.5%w/w in solution before filtration). It is composed from the following scattering contributions: $I_{\mathrm{FF}}(q)$ (blue line, Eq. (A.3)), the spherical form factor integrated over a log-normal distribution $p_z(R)$; the Teubner-Strey component $I_{\mathrm{TS}}(q)$ (red line) standing for intra-particles electron density fluctuations and the X-ray background (green line).

Regarding the structure factor $S(q)$, we systematically used same parameters as the ones found for the form factor $P(q)$ (particles radius R and their volume fraction) and we do not expect a strong contribution to the total intensity because of the low particles concentrations studied ($S(q) \sim 1, \forall q$).

We focus now on the scattered intensity expected for BSA proteins solutions. At pH 7, low ionic strength (I<0.3 M) and low concentrations, the BSA is often described as a monomolecular oblate spheroid [24,25]. An oblate spheroid results from an ellipse revolved about its shorter (minor) axis, producing a surface that is flattened at the poles and wider at the equator. The form factor of spheroids as been described by Guinier [23] and is written as:

$$P(q) = \int_0^1 \left|\frac{3(\sin u - u\cos u)}{u^3}\right|^2 \mathrm{d}x \tag{A.18}$$

with:

$$u = q\sqrt{r_p^2 x^2 + r_e^2(1-x^2)} \tag{A.19}$$

where r_p and r_e are the principal (or polar) and equatorial semi-axes, respectively. To compute the scattering intensity $I(q)$, the form factor is

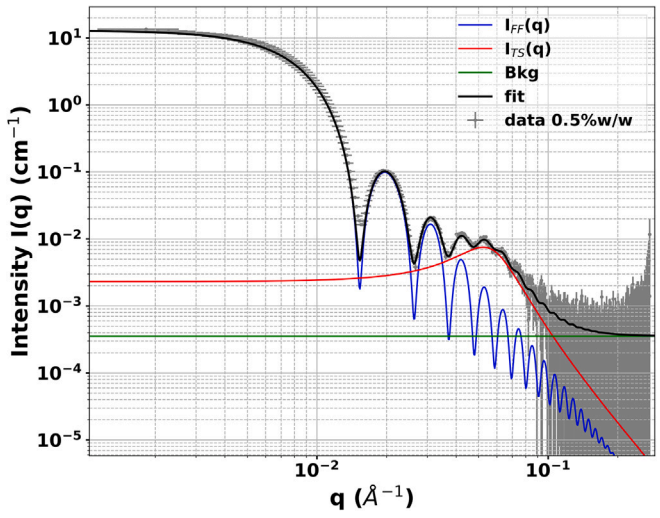

Fig. A.7. SAXS 1D intensity curve measured for PE batch sample at 0.5%w/w (in gray). The best fit to the data is the black line and is composed by summation of the form factor contribution $I_{FF}(q)$ in blue, the Teubner-Strey model $I_{TS}(q)$ in red and the background level *Bkg* in green.

multiplied by the square of the scattering length density contrast $\Delta(\rho b)$ and the square of the particles volume $V = \frac{4}{3}\pi r_e^2 r_p$.

When analyzing diluted solutions of mixture of PE-NPs/BSA, we considered three models composed of added intensity contributions [in cm^{-1}]: (1) the form and structure factor of a sphere using a log-normal distribution function of the radius (PE-NPs), the Teubner-Strey broad correlation peak, the form factor of a spheroid (free BSA proteins) and a constant background. (2) a core–shell-box form factor with a core corresponding to PE-NPs and a shell corresponding to adsorbed BSA proteins, the Teubner-Strey model, the form factor of a spheroid (non-adsorbed BSA proteins) and a background level. (3) the profiled-core–shell form factor (core=PE-NPs, shell=BSA corona including BSA amino-acids and water), the Teubner-Strey model, the form factor of a spheroid (non-adsorbed BSA proteins) and a background level.

The core–shell-box form factor is often used to describe a uniform shell density around a spherical core. It assumes two heavy-side interfaces of the scattering profile (core/shell and shell/solvent), and writes:

$$\tilde{P}(\vec{q}) = P(\vec{q})/(\Delta\left(\rho b_{\text{core/shell}}\right) V_{\text{core}} + \Delta\left(\rho b_{\text{shell/solv}}\right) V_{\text{shell}})^2 \tag{A.20}$$

$$\text{with} \quad P(\vec{q}) = \left(\frac{3V_{\text{core}}\Delta\left(\rho b_{\text{core/shell}}\right) j_1(qR_{\text{core}})}{qR_{\text{core}}} + \frac{3V_{\text{shell}}\Delta\left(\rho b_{\text{shell/solv}}\right) j_1(qR_{\text{shell}})}{qR_{\text{shell}}} \right)^2 \tag{A.21}$$

$$\text{and} \quad j_1(x) = (\sin x - x\cos x)/x^2 \tag{A.22}$$

The profiled-core–shell corresponds to the situation where a spherical particle is surrounded by a shell including a contrasted molecule (BSA corona) and a solvent profile. The form factor includes three interface contributions (core/solvent, solvent/shell, shell/solvent), noting their locations with respect to the core center R and their roughnesses σ, we have [26–28,47][1]:

$$P_{\text{core,sh}}\left(q, W_{\text{core}}, \sigma_{\text{core}}, D, \sigma_{\text{sh,in}}, W_{\text{sh}}, \sigma_{\text{sh,out}}\right) = \left(\Delta(\rho b_{\text{shell/solv}})\right) F\left(q, R_{\text{out}}, \sigma_{\text{out}}\right) + \left(\Delta(\rho b_{\text{solv/shell}})\right) F\left(q, R_{\text{sh,in}}, \sigma_{\text{sh,in}}\right) + \left(\Delta(\rho b_{\text{core/solv}})\right) F\left(q, R_{\text{core}}, \sigma_{\text{core}}\right) \tag{A.23}$$

[1] The model used was adapted from the one descried in the SASfit software documentation.

with W_{core} and W_{sh} the radius of the core and shell, respectively, separated by the distance D. Roughness is included via parabolic functions, σ_{core} is the roughness of the core/solvent(layer) interface, $\sigma_{\text{sh,in}}$ is the roughness of the solvent(layer)/shell interface and σ_{out} is the roughness of the shell/solvent(bulk) interface. All interfaces are located with respect to the core center with: $R_{\text{core}} = W_{\text{core}} + \sigma_{\text{core}}$, $R_{\text{sh,in}} = R_{\text{core}} + D$ and $R_{\text{out}} = R_{\text{sh,in}} + \sigma_{\text{sh,in}} + W_{\text{sh}} + \sigma_{\text{out}}$ (all parameters are shown in Fig. A.8). $F(q, R, \sigma)$ corresponds to the contribution of each interface to the form factor such as:

$$F(q,R,\sigma) = 4\pi\left(\left(\frac{R}{\sigma^2}+\frac{1}{\sigma}\right)\frac{\cos(q(R+\sigma))}{q^4} + \left(\frac{R}{\sigma^2}-\frac{1}{\sigma}\right)\frac{\cos(q(R-\sigma))}{q^4} - 3\frac{\sin(q(R+\sigma))}{q^5\sigma^2} - 3\frac{\sin(q(R-\sigma))}{q^5\sigma^2} + 6\frac{\sin(qR)}{q^5\sigma^2} - 2R\frac{\cos(qR)}{q^4\sigma^2}\right) \tag{A.24}$$

It also corresponds to the Fourier transform of the radial profile which is given by:

$$\varsigma(r,R,\sigma) = \begin{cases} 1 & \text{for } r \le R-\sigma \\ 1 - \frac{1}{2}\frac{(r-R+\sigma)^2}{\sigma^2} & \text{for } R-\sigma < r \le R \\ \frac{1}{2}\frac{(R-r+\sigma)^2}{\sigma^2} & \text{for } R < r \le R+\sigma \\ 0 & \text{for } r > R+\sigma \end{cases} \tag{A.25}$$

The total scattering length density profile $\rho b(r)$ can be calculated as follow:

$$\rho b(r) = \left(\rho b_{\text{core}} - \rho b_{\text{solv}}\right)\varsigma(r, R_{\text{core}}, \sigma_{\text{core}}) + \left(\rho b_{\text{solv}} - \rho b_{\text{shell}}\right)\varsigma(r, R_{\text{sh,in}}, \sigma_{\text{sh,in}}) + + \left(\rho b_{\text{shell}} - \rho b_{\text{solv}}\right)\varsigma(r, R_{\text{out}}, \sigma_{\text{out}}) + \rho b_{\text{solv}} \tag{A.26}$$

The Fig. A.9 presents the full decomposition of all scattering components to the fit corresponding to the mixture at $X = V_{\text{BSA}}/V_{\text{PE-NP}}$=1.63 with V_{BSA} and $V_{\text{PE-NP}}$ the volumes of BSA and PE-NPs at same concentration of 0.37%w/w (or PPMR=864 with PPMR $= X M_{\text{w,NP}}/M_{\text{w,BSA}}$, with $M_{\text{w,NP}}$ and $M_{\text{w,BSA}}$ corresponding to the molecular weights of the PE-NPs and BSA, respectively). Thus, one can see how the contribution from the free BSA proteins in solution contributes to the total scattered intensity. The cyan line corresponds to the scattering contribution due to the NPs coated with BSA and is equal to the sum of the scattering from the profiled-core–shell model ($I_{\text{NP+BSA}}(q)$, in blue) and the scattering from the Teubner-Strey model ($I_{\text{TS}}(q)$, in red). The free BSA contribution corresponds to the orange line using the parameters from the fit of the pure BSA solution so that the only parameter fitted for this component here is the volume fraction of free BSA that differs from the BSA batch solution. The scattering from the free BSA proteins reduces drastically the depth of the oscillations measured from a pure PE nanoparticles solution but several fringes remain well defined and are properly fitted with the profiled-core–shell form factor. This last contribution is the only one that can account for a shift in the oscillations period.

Appendix B. Fitting procedure for SAXS

We described in great details all the models used for modeling the SAXS data. In this section, we describe some features about the way we conducted the different fits. We first present the fitting procedure used for the SAXS data measured from pure PE-NPs and then the one used for the mixture PE-NPs/BSA.

B.1. Pure PE-NPs solutions

To fit the pure PE-NPs SAXS intensities, we sum the intensity coming from the spherical form factor $P(q)$, the Teubner-Strey contribution and a background level (residual scattering remaining after the data treatment to reach absolute scale intensity 1D-SAXS curves). Regarding the spherical form factor, the parameters to fit are: $\Phi_{\text{v,PE}}$, μ_R, σ_R, ρb_{core} and ρb_{solvent}. For the Teubner-Strey contribution, we have three parameters: ξ, D^* and η_{TS} (corresponding to the term $\langle \Phi_{\text{v}}(1-\Phi_{\text{v}})(\Delta(\rho b))^2 \rangle$) and lastly for the constant background (independent of q) we only have one fitted parameter. We got nine parameters to fit per curve

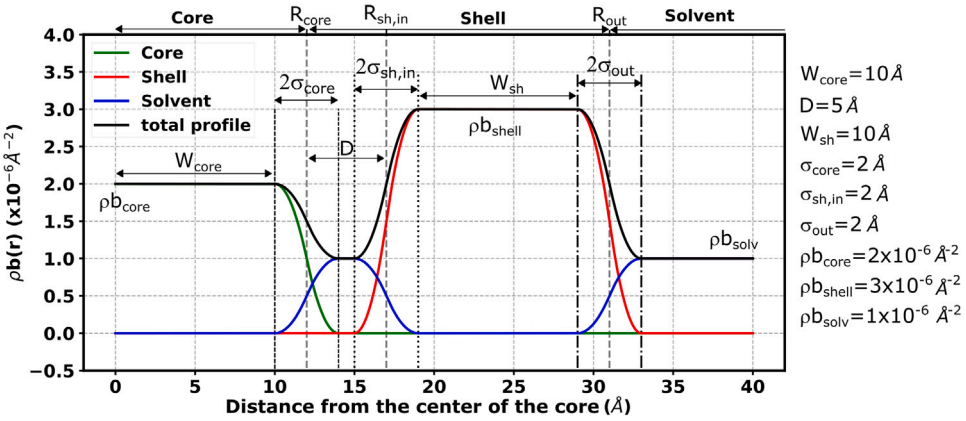

Fig. A.8. Schematic representation of the radial scattering length density profile using the profiled-core–shell model with the location of all interfaces (R_{core}, $R_{sh,in}$, R_{out}), thicknesses (W_{core}, D, W_{sh}) and roughnesses (σ_{core}, $\sigma_{sh,in}$, σ_{out}). The parameters used are shown on the right of the figure.

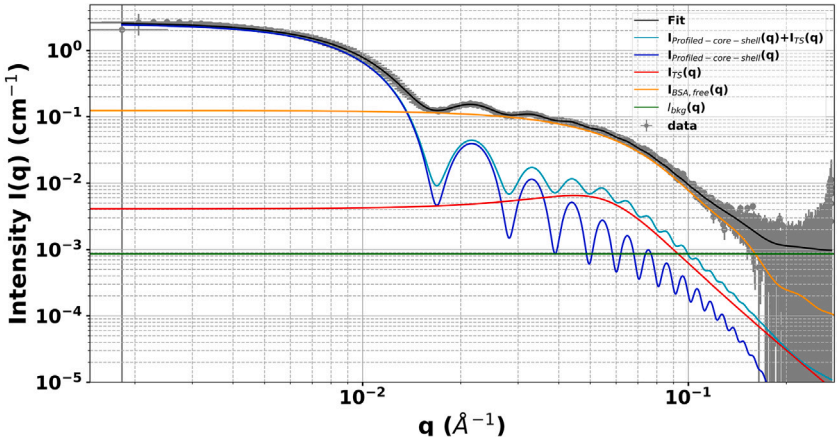

Fig. A.9. Decomposition showing all different contributions to the total SAXS intensity fitted for a mixture of BSA proteins and PE nano-particles at mixing ratio PPMR=864 (X=1.63) in PB 10 mM at pH=7.2. Data points are plotted with their error bars in gray, the best fit corresponds to the black line and corresponds to the sum of: the contribution of the profiled-core–shell contribution of NP-BSA ($I_{\text{profiled-core–shell}}(q)$, blue line), the correlation peak of the NP described by the Teubner-Strey model ($I_{TS}(q)$, red line), the free BSA in solution ($I_{BSA}(q)$, orange line) and the background level ($I_{bkg}(q)$, green line). We also present the curve that would be obtained neglecting the free BSA proteins in solution and in absence of background ($I_{\text{profiled-core–shell}}(q) + I_{TS}(q)$, cyan line).

with correlated parameters, therefore fits should be done carefully. Thus, we fitted data measured at different concentrations and fitted the parameters that are independent of the concentration simultaneously for all data and for this we used a homemade Python fitting program. For example, for a set of curves at different concentrations, we imposed common fitting parameters: μ_R, σ_R, ρb_{core} and ρb_{solvent}, ξ, D^*. The volume fractions are fitted independently for each curve and used to recalculate the dilution factors. The Teubner-Strey scattering peak is proportional to the PE volume fraction in solution, therefore we used the parameter η_{TS} that controls the Teubner-Strey scattering intensity and linked it to the changes in nanoparticles concentration. So, η_{TS} scales with concentrations in the fits by the dilution factor. The constant residual background is fitted for each curve.

To check that we properly took into account all contributions and the instrumental resolution effects (smearing), we then reused the set of the best fitted parameters obtained from our homemade program into SASfit software to check that we obtain same parameters using its fitting algorithms.

B.2. PE-NPs/BSA mixture solutions

To fit the SAXS data from the PE-NPs/BSA mixtures, as described earlier, we used the sum of the profiled-core–shell form factor, a Teubner-Strey contribution, a spheroid form factor for the free BSA in solution and a constant residual background level. In this case, we only used the SASfit software to fit the data since it is quite convenient.

We also faced the fact that some parameters are correlated with others in the different contributions to the total scattering intensity. Parameters are also linked between different SAXS data curves (at different PPMR for the mixtures of PE-NPs/BSA prepared from the same batch solutions). Therefore, we fixed several parameters to the value obtained while we fitted data that were strongly affected the fit quality (χ^2 sensitive to the parameters). Then, we systematically checked that when released, they stayed very close to the value fixed. In that way for instance, at extremely low concentrations of added BSA to the PE nanoparticles, we could fix the free BSA form factor parameters, to the ones measured in pure BSA solutions. This approach drastically reduces the calculation time of the fitting algorithm and enhances the consistency of set of parameters obtained from same batches. As seen previously, we could fix: μ_R, σ_R, ρb_{core} and ρb_{solvent}, ξ, D^* concerning the PE-NPs, and for the contribution of BSA free in solution ρb_{BSA}, and its size parameters r_p and r_e (given by the fit of pure BSA SAXS curve). We also noticed that the thin layer of solvent at the core/shell interface, as well as all shell roughnesses, did not evolved drastically between fits and could be fixed to a mean value for all samples. Nevertheless, the model needs such parameters to get a lower χ^2 value that attests for a slightly better fit quality. Also, water is expected in the shell, with adsorbing BSA proteins to the PE core.

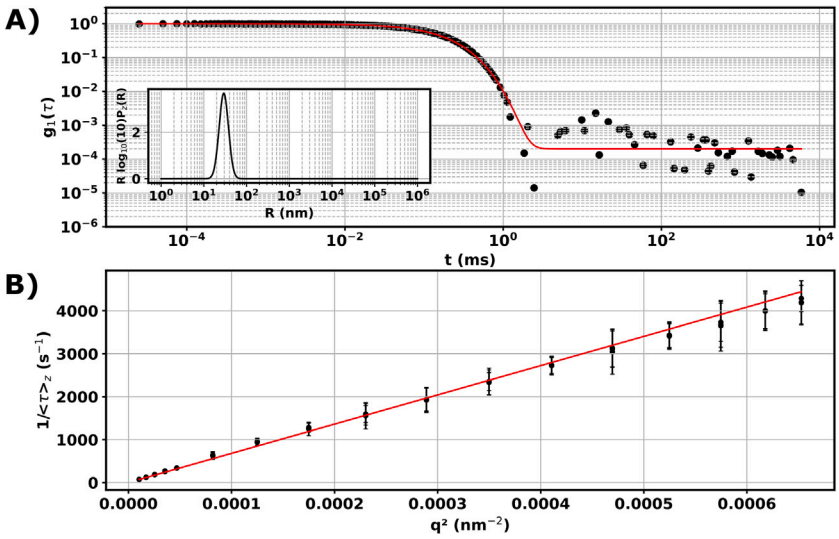

Fig. C.10. (A) Autocorrelation function of DSP-PE-NPs batch sample at 0.1%w/w, measured at 90 ° for 30 s. The red curve represents the fit deduced from the unique radius distribution fitted from all the measurements at all angles, which is drawn within the inset. (B) Plot of the mean frequencies deduced from CONTIN algorithm versus q^2 at 0.1%w/w. The linear fit result is plotted with the red line.

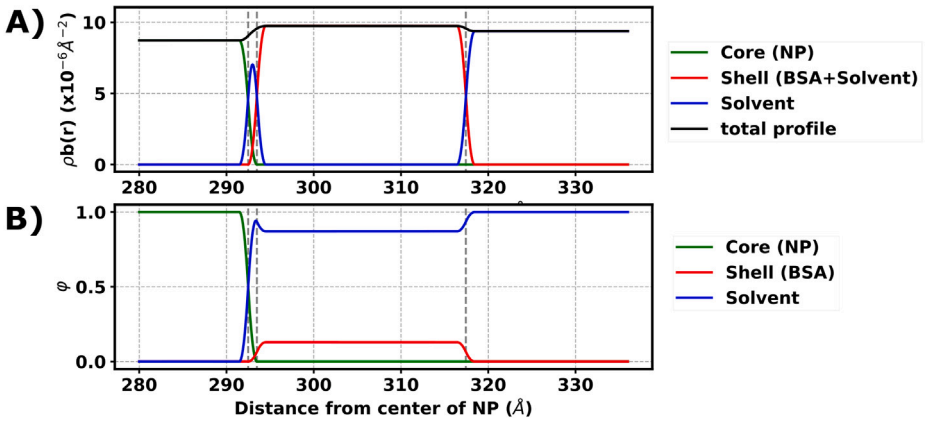

Fig. D.11. (A) Scattering length density profiles plotted as a function of the distance from the center of the nanoparticle for: the PE core (green line), the hydrated shell (red line), the solvent (blue line) and the total one (black line). (B) Void fraction profiles with respect to the nanoparticle core center for the PE core (green line), the BSA (red line) and the solvent (blue line). For both plots: the gray vertical lines represent, from left to right, the positions of R_{core}, $R_{sh,in}$ and R_{out}.

We generally obtained values around 1 Å and we do not consider that we are establishing a good measurement of these precise values. To the end, the most effective approach was to fit: the volume fractions $\Phi_{v,PE}$ and $\Phi_{v,BSA}$, the shell scattering length density ρb_{shell}, the shell thickness W_{sh}, the Teubner-Strey η_{TS} parameter keeping it proportional to the nanoparticles concentration and the background constant.

B.3. Isotherms confidence intervals and uncertainties

As reported earlier, the fitting model comes with non linearly correlated parameters and some were fixed when the model is poorly sensitive to their precise value. Therefore, determination of uncertainties were difficult to estimate quantitatively. As a consequence, the uncertainties of the isotherm cannot be ascertained directly from the SAXS fitting algorithm or from linear combinations of the uncertainties from fitting parameters. As a useful guide to the eyes, we decided to plot confidence-bars for each point, rather than statistical error-bars, using the following procedure:

- Data confidence intervals for the *y*-axis (plotted as vertical black bars on the *y*-axis for all points of the isotherm, expressed in mg.m^{-2}): while the fit has converged to the best set of parameters for a sample, we obtain a reduced χ^2 value corresponding to its best fit. The fitted ρb_{shell} parameter is then varied to smaller and larger values, so that χ^2 did not vary by more than 10% from its original value (positively and negatively around the best fit value). From the two extreme values of ρb_{shell}, we calculated the corresponding adsorbed BSA mass. In this way, we determine the vertical (top and bottom) intervals of confidence for each isotherm data point, corresponding to a precise fitted SAXS curve and sample.
- Data confidence intervals for the *x*-axis (plotted as horizontal black bars on the *x*-axis for all points of the isotherm, expressed in mg.mL^{-1}): (1) the left value of the confidence-bar is obtained as explained here: from the best fit to the SAXS curve corresponding to a point of the isotherm, we subtracted to the measured SAXS curve, all fitted contributions except the fitted free BSA SAXS contribution curve. Thus, the remaining SAXS intensity curve, corresponds now to the SAXS data which is fitted for the free BSA spheroid form factor. As the free BSA concentration is a fitting parameter of this free BSA spheroid contribution (via the free BSA volume fraction, $\Phi_{v,BSA}$), we determined the left confidence bar by decreasing its value to obtain the minimum amount of free

Table E.1
Fitted parameters found for BSA and DSP-PE-NPs mixtures at different concentration ratio. The other parameters were kept constant at: $\sigma_{R,z}$=0.02, $R_{mean,PE}$=29.2 nm, $\sigma_{core} = \sigma_{sh,in} = \sigma_{out}$=1 Å, D=1 Å, ρb_{core}=8.720 × 10^{-6} $Å^{-2}$, ρb_{solv}=9.373 × 10^{-6} $Å^{-2}$, ξ=60.9 Å, $D*$=115.0 Å, r_p=18.9 Å, r_e=44.4 Å, ρb_{BSA}=1.223 × $10^{-5}Å^{-2}$, the parameter $N_{v,BSA}$ is related to $\Phi_{v,BSA}$ by the relation $N_{v,BSA} = \Phi_{v,BSA} \times 10^8 / V_{1BSA}$.

Form factor PE (microgel core–shell)			Teubner strey	Background	Form factor BSA
$\Phi_{v,PE}$	W_{sh} (Å)	ρb_{shell} ($Å^{-2}$)	η_{TS} ($Å^{-3/2}$ $cm^{-1/2}$)	Bkg (cm^{-1})	$N_{v,BSA}$
2.07×10^{-3}	1.02	9.690×10^{-6}	1.98×10^{-4}	3.62×10^{-4}	0.03
3.30×10^{-3}	30.42	9.475×10^{-6}	2.50×10^{-4}	4.59×10^{-4}	0.03
3.38×10^{-3}	30.85	9.484×10^{-6}	2.61×10^{-4}	7.45×10^{-4}	0.01
3.18×10^{-3}	28.23	9.523×10^{-6}	2.46×10^{-4}	5.20×10^{-4}	0.05
3.11×10^{-3}	26.87	9.506×10^{-6}	2.48×10^{-4}	2.43×10^{-4}	0.02
3.13×10^{-3}	24.50	9.586×10^{-6}	2.44×10^{-4}	3.97×10^{-4}	0.08
2.71×10^{-3}	29.32	9.552×10^{-6}	2.26×10^{-4}	7.28×10^{-4}	0.07
2.16×10^{-3}	27.07	9.784×10^{-6}	2.17×10^{-4}	7.64×10^{-4}	0.41
1.86×10^{-3}	30.10	9.739×10^{-6}	1.97×10^{-4}	8.60×10^{-4}	0.41
1.05×10^{-3}	29.87	9.852×10^{-6}	1.91×10^{-4}	9.47×10^{-4}	0.80

Table E.2
Calculated intermediate variables deduced from the fitted parameters found for mixtures of BSA and DSP-PE-NPs at different concentration ratio to plot the adsorption isotherm.

C_{PE} (mg/mL)	V_{shell} (m^3)	$N_{BSA,max}$	N_{BSA} in shell	m_{ads} (mg/m^2)	$\Phi_{v,BSA}$	$C_{BSA,free}$ (mg/mL)
2.01	2.06×10^{-24}	14.61	1.62	0.02	4.38×10^{-5}	0.06
3.21	3.69×10^{-23}	262.33	9.29	0.10	4.08×10^{-5}	0.05
3.28	3.75×10^{-23}	266.37	10.30	0.11	1.82×10^{-5}	0.02
3.08	3.41×10^{-23}	242.23	12.71	0.13	8.49×10^{-5}	0.11
3.02	3.24×10^{-23}	229.92	10.71	0.11	3.66×10^{-5}	0.05
3.03	2.94×10^{-23}	208.60	15.51	0.16	1.26×10^{-4}	0.17
2.63	3.55×10^{-23}	252.19	15.75	0.16	1.13×10^{-4}	0.15
2.09	3.26×10^{-23}	231.75	33.32	0.35	6.35×10^{-4}	0.84
1.80	3.65×10^{-23}	259.37	33.16	0.34	6.39×10^{-4}	0.84
1.02	3.62×10^{-23}	257.25	43.05	0.45	1.25×10^{-3}	1.66

Table E.3
Fitted parameters found for BSA and Bare-PE-NPs mixtures at different concentration ratio. The other parameters were kept constant at: $\sigma_{R,z}$=0.01, $R_{mean,PE}$=32.3 nm, $\sigma_{core} = \sigma_{sh,in} = \sigma_{out}$=1 Å, D=1 Å, ρbcore=8.976 × 10^{-6} $Å^{-2}$, ρb_{solv}=9.373 × 10^{-6} $Å^{-2}$, ξ=35.2 Å, $D*$=120.3 Å, r_p=19.2 Å, r_e=43.6 Å, ρb_{BSA}=1.259 × 10^{-5} $Å^{-2}$, the parameter $N_{v,BSA}$ is related to $\Phi_{v,BSA}$ by the relation $N_{v,BSA} = \Phi_{v,BSA} \times 10^8 / V_{1BSA}$.

Form factor PE (microgel core–shell)			Teubner strey	Background	Form factor BSA
$\Phi_{v,PE}$	W_{sh} (Å)	ρb_{shell} ($Å^{-2}$)	η_{TS} ($Å^{-3/2}$ $cm^{-1/2}$)	Bkg (cm^{-1})	$N_{v,BSA}$
5.11×10^{-3}	24.63	9.384×10^{-6}	3.47×10^{-4}	1.00×10^{-5}	0.01
5.38×10^{-3}	29.99	9.390×10^{-6}	3.61×10^{-4}	4.75×10^{-5}	0.01
5.38×10^{-3}	33.53	9.405×10^{-6}	3.72×10^{-4}	1.99×10^{-5}	0.02
5.11×10^{-3}	36.65	9.398×10^{-6}	3.31×10^{-4}	8.28×10^{-5}	0.04
5.29×10^{-3}	44.99	9.414×10^{-6}	3.60×10^{-4}	9.85×10^{-5}	0.03
5.12×10^{-3}	49.98	9.427×10^{-6}	3.49×10^{-4}	4.75×10^{-5}	0.05
5.01×10^{-3}	47.64	9.418×10^{-6}	3.34×10^{-4}	1.99×10^{-5}	0.06
5.01×10^{-3}	49.86	9.446×10^{-6}	3.30×10^{-4}	6.82×10^{-5}	0.08
4.71×10^{-3}	58.38	9.442×10^{-6}	3.20×10^{-4}	1.99×10^{-5}	0.12
4.37×10^{-3}	55.36	9.467×10^{-6}	3.05×10^{-4}	4.90×10^{-4}	0.15
2.88×10^{-3}	57.14	9.612×10^{-6}	2.09×10^{-4}	8.39×10^{-4}	0.47
1.96×10^{-3}	65.91	9.676×10^{-6}	1.07×10^{-4}	4.79×10^{-4}	0.64
1.32×10^{-3}	58.69	9.746×10^{-6}	9.72×10^{-5}	9.98×10^{-4}	0.80
6.95×10^{-4}	54.51	9.780×10^{-6}	5.00×10^{-5}	9.60×10^{-4}	0.91
3.36×10^{-4}	63.54	9.713×10^{-6}	1.10×10^{-5}	9.88×10^{-4}	0.97

BSA which is needed to fill the minima of the particles form factor oscillations; (2) the right value of the confidence-bar is simply the value corresponding to the known total amount of BSA that was used to prepare this sample. So, it marks an absolute limit for the maximum amount of free BSA that could be found for this sample in the extreme case where no interactions take place with the PE nanoparticles.

Appendix C. Multi-angle light scattering results

To confirm the particle size obtained from SAXS experiments, we also performed multi-angle light scattering (MALS) experiments. We recall that for MALS experiments, we measure the autocorrelation curve of scattered coherent light as a function of a relaxation time (often called $g_2(\vec{q},\tau)$) at different scattering angles. We work here on the autocorrelation function $g_1(\vec{q},\tau)$ related to $g_2(\vec{q},\tau)$ by the Siegert relationship: $g_2(\vec{q},\tau)=1+\beta(g_1(\vec{q},\tau))^2$. In a log–log scale, $g_1(\vec{q},\tau)$ has a plateau at $\tau \to 0$, then the curve decreases to reach a noise level. This curve can be expressed as:

$$g_1(\vec{q},\tau) = \frac{\int_0^\infty \exp(-t/\tau)\, \tilde{P}(\vec{q})\tilde{p}_z(\tau)\mathrm{d}\tau}{\int_0^\infty \tilde{P}(\vec{q})\tilde{p}_z(\tau)\mathrm{d}\tau} \quad \text{(C.1)}$$

With $\tilde{P}(\vec{q})$ the normalized form factor (hard sphere here) and $\tilde{p}_z(\tau)$ the normalized z-averaged relaxation time distribution (log-normal). $\tilde{p}_z(\tau)$

Table E.4
Calculated intermediate variables deduced from the fitted parameters found for mixtures of BSA and Bare-PE-NPs at different concentration ratio to plot the adsorption isotherm.

C_{PE} (mg/mL)	V_{shell} (m^3)	$N_{BSA,max}$	N_{BSA} in shell	m_{ads} (mg/m^2)	$\Phi_{v,BSA}$	$C_{BSA,free}$ (mg/mL)
4.95	3.49×10^{-23}	247.99	0.83	0.01	1.97×10^{-5}	0.03
5.22	4.32×10^{-23}	306.57	1.62	0.01	1.61×10^{-5}	0.02
5.22	4.88×10^{-23}	346.18	3.45	0.03	2.30×10^{-5}	0.03
4.96	5.38×10^{-23}	381.86	2.93	0.02	6.74×10^{-5}	0.09
5.13	6.76×10^{-23}	480.19	6.08	0.05	4.91×10^{-5}	0.06
4.96	7.62×10^{-23}	541.26	9.11	0.08	7.76×10^{-5}	0.10
4.86	7.22×10^{-23}	512.39	7.10	0.06	9.57×10^{-5}	0.13
4.86	7.60×10^{-23}	539.75	12.12	0.10	1.20×10^{-4}	0.16
4.56	9.12×10^{-23}	647.73	13.74	0.12	1.83×10^{-4}	0.24
4.24	8.58×10^{-23}	608.94	17.71	0.15	2.29×10^{-4}	0.30
2.80	8.90×10^{-23}	631.72	46.97	0.40	7.21×10^{-4}	0.95
1.90	1.05×10^{-22}	747.22	70.35	0.59	9.74×10^{-4}	1.29
1.28	9.18×10^{-23}	651.74	75.52	0.64	1.23×10^{-3}	1.62
0.67	8.42×10^{-23}	598.04	75.57	0.64	1.39×10^{-3}	1.83
0.33	1.01×10^{-22}	715.50	75.58	0.64	1.49×10^{-3}	1.97

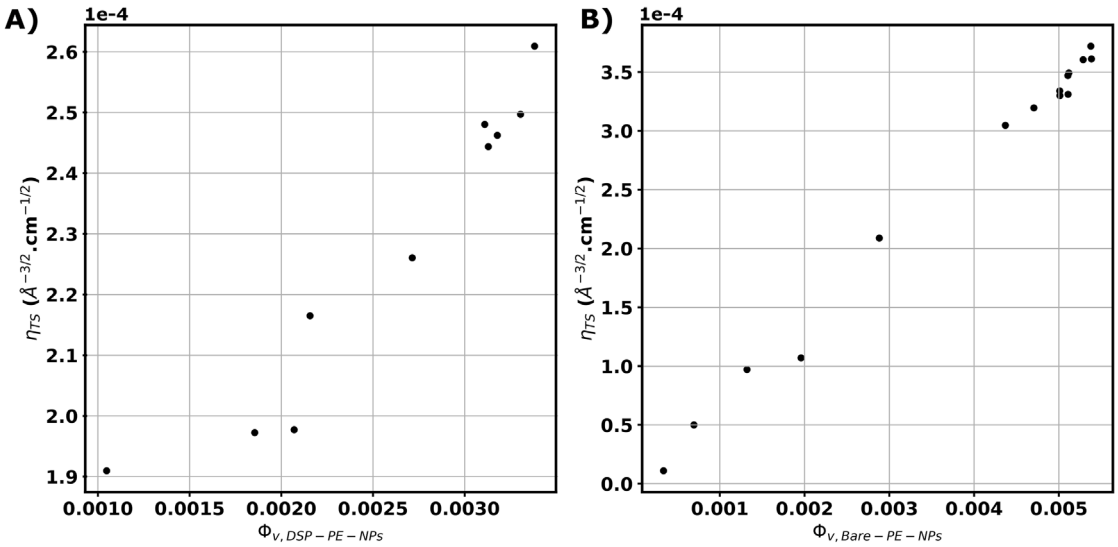

Fig. E.12. Figure of the Teubner-Strey parameter η_{TS} as a function of the PE-NPs volume fraction for the DSP-PE-NPs (figure A) and the Bare-PE-NPs (figure B) experiences.

related to the hydrodynamic radii distribution by: $\tilde{p}_z(R_H) = \frac{6\pi\eta}{q^2 k_B T}\tilde{p}_z(\tau)$, with η the dynamic viscosity, k_B the Boltzmann constant, and T the temperature.

For MALS measurements, the autocorrelation curves are measured at several angles in order to take into account the fact that the scattering intensity changes with angle depending on the size distribution (*i.e.* big objects scatter more than smaller ones at small $\vec{q}$). Here, we measured from 14° to 150°, 3 times per angles, 30 s for each measurement and at several concentrations. We only present here the results measured at 0.1%w/w concentration.

To analyze the data, we considered two different approaches. The first one is to consider one unique size distribution that fits all the data collected at all angles. This has been done using a homemade program that fits all curves with a unique set of parameters for $\tilde{p}_z(R_H)$, taking into account the effects related to the measured angle for each curve. We present in Fig. C.10-A) one of the autocorrelation functions measured at 90° and the corresponding fit that considers all the other measurements as well. The best fit size distribution obtained is shown in the inset and is calculated from the following parameters: μ_{R_H}=29.3 nm and σ_{R_H}=0.25.

The second procedure uses the well-known CONTIN algorithm that gives several solutions of the relaxation time distribution $\tilde{p}_z(\tau)$, depending on the regularization parameter used (often named α). Usually, a best solution is chosen when a good balance between the smoothness of the distribution and the goodness of the fit is found. Instead of doing this, we explore all the solutions found at a given angle to get the closest result between the three measurements made. In other words, we are looking for the best consistency between the measurements made at the same angle since the same objects scatter, so same distribution should be found. From this, we extract a relaxation time distribution and its different momenta. Considering the first momentum, we get the mean relaxation time $\langle\tau\rangle_z$ that is linear with q^{-2} as:

$$\frac{1}{\langle\tau\rangle_z} = \frac{k_B T}{6\pi\eta}\frac{1}{\langle R_H\rangle_z}q^2 \tag{C.2}$$

We applied this procedure for all the measurements at all angles and we obtained the linear behavior shown in Fig. C.10-B). In addition to this linear behavior of the frequency with q^2, we also see that each mean relaxation frequency at the same angle is very close. The uncertainties are obtained from the second momentum. A linear fit of this curve provides a z-averaged hydrodynamic radius of $\langle R_H\rangle_z$=30.9 ± 0.3 nm, which is consistent with the previous method.

Appendix D. Complementary figure of protocol 1

See Fig. D.11.

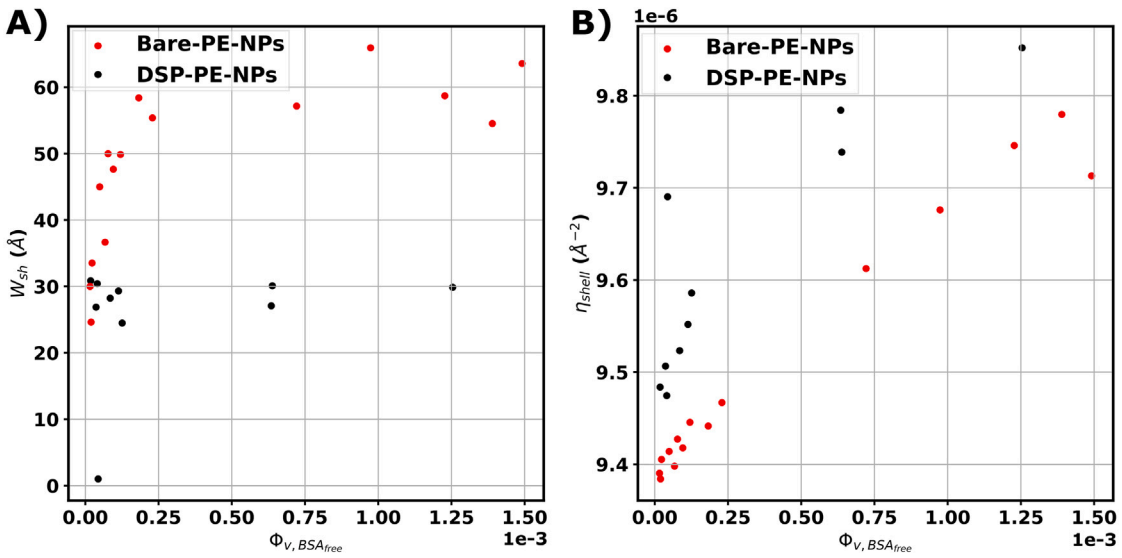

Fig. E.13. (A) Figure of the fitted shell thickness depending on the free BSA volume fraction in solution for both Bare and DSP-PE-NPs exposed to BSA. (B) Figure of the fitted scattering length density of the shell as a function of the free BSA volume fraction.

Appendix E. Complementary figures of protocol 2

See Fig. E.12, Fig. E.13 and Tables E.1–E.4.

Appendix F. Supplementary data

Supplementary material related to this article can be found online at https://doi.org/10.1016/j.colsurfa.2026.139961.

Data availability

Data will be made available on request.

References

[1] R. Geyer, J.R. Jambeck, K.L. Law, Production, use, and fate of all plastics ever made, Sci. Adv. 3 (7) (2017) e1700782.
[2] T. Zhang, Z. Wang, Y. Wu, S. Zhu, J. Su, Interactions of micro-and nanoplastics with biomolecules: from public health to protein corona effect and beyond, J. Phys. Chem. B (2025).
[3] J. Gigault, B. Pedrono, B. Maxit, A. Ter Halle, Marine plastic litter: the unanalyzed nano-fraction, Environ. Sci.: Nano 3 (2) (2016) 346–350.
[4] M.S.-L. Yee, L.-W. Hii, C.K. Looi, W.-M. Lim, S.-F. Wong, Y.-Y. Kok, B.-K. Tan, C.-Y. Wong, C.-O. Leong, Impact of microplastics and nanoplastics on human health, Nanomaterials 11 (2) (2021) 496.
[5] K. Tallec, O. Blard, C. González-Fernández, G. Brotons, M. Berchel, P. Soudant, A. Huvet, I. Paul-Pont, Surface functionalization determines behavior of nanoplastic solutions in model aquatic environments, Chemosphere 225 (2019) 639–646.
[6] I. Paul-Pont, K. Tallec, C. Gonzalez-Fernandez, C. Lambert, D. Vincent, D. Mazurais, J.-L. Zambonino-Infante, G. Brotons, F. Lagarde, C. Fabioux, et al., Constraints and priorities for conducting experimental exposures of marine organisms to microplastics, Front. Mar. Sci. 5 (2018) 252.
[7] E. Grau, P.-Y. Dugas, J.-P. Broyer, C. Boisson, R. Spitz, V. Monteil, Aqueous Dispersions of Nonspherical Polyethylene Nanoparticles from Free-Radical Polymerization under Mild Conditions, Angew. Chem. Int. Ed. 49 (38) (2010) 6810–6812.
[8] G. Billuart, E. Bourgeat-Lami, M. Lansalot, V. Monteil, Free radical emulsion polymerization of ethylene, Macromolecules 47 (19) (2014) 6591–6600.
[9] S. Liu, M. Junaid, H. Liao, X. Liu, Y. Wu, J. Wang, Eco-corona formation and associated ecotoxicological impacts of nanoplastics in the environment, Sci. Total Environ. 836 (2022) 155703.
[10] X. Shi, Z. Chen, W. Wei, J. Chen, B.-J. Ni, Toxicity of micro/nanoplastics in the environment: Roles of plastisphere and eco-corona, Soil Environ. Health 1 (1) (2023) 100002.
[11] F. Barraqué, M.A. Fernández, F.S. García Einschlag, F.M. Flores, Adsorption of bovine serum albumin on magnetic material montmorillonite: Isotherms, kinetic, thermodynamic, and mechanism studies, Arab. J. Sci. Eng. 49 (7) (2024) 9367–9379.
[12] S. Shourni, A. Javadi, N. Hosseinpour, A. Bahramian, M. Raoufi, Characterization of protein corona formation on nanoparticles via the analysis of dynamic interfacial properties: Bovine serum albumin - silica particle interaction, Colloids Surfaces A: Physicochem. Eng. Asp. 638 (2022) 128273.
[13] X. Li, E. He, K. Jiang, W.J. Peijnenburg, H. Qiu, The crucial role of a protein corona in determining the aggregation kinetics and colloidal stability of polystyrene nanoplastics, Water Res. 190 (2021) 116742.
[14] R.D. Avellán-Llaguno, X. Zhang, P. Zhao, A. Velez, M. Cruz, J. Kikuchi, S. Dong, Q. Huang, Differential aggregation of polystyrene and titanium dioxide nanoparticles under various salinity conditions and against multiple proteins types, Environ. Sci. Pollut. Res. 29 (49) (2022) 74173–74184.
[15] S. Kihara, S. Ghosh, D.R. McDougall, A.E. Whitten, J.P. Mata, I. Köper, D.J. McGillivray, Structure of soft and hard protein corona around polystyrene nanoplastics—Particle size and protein types, Biointerphases 15 (5) (2020).
[16] S. Yu, A. Perálvarez-Marín, C. Minelli, J. Faraudo, A. Roig, A. Laromaine, Albumin-coated SPIONs: An experimental and theoretical evaluation of protein conformation, binding affinity and competition with serum proteins, Nanoscale 8 (30) (2016) 14393–14405.
[17] F.E. Galdino, A.S. Picco, L.B. Capeletti, J. Bettini, M.B. Cardoso, Inside the protein corona: From binding parameters to unstained hard and soft coronas visualization, Nano Lett. 21 (19) (2021) 8250–8257.
[18] L. Marichal, Interactions Protéines-Nanoparticules : émergence de Nouveaux Facteurs Déterminant la Formation de la Couronne de Protéines (Ph.D. thesis), (2018SACLS100) Université Paris Saclay (COmUE), 2018.
[19] L.F. Ferreira, A.S. Picco, F.E. Galdino, L.J.C. Albuquerque, J.-F. Berret, M.B. Cardoso, Nanoparticle–protein interaction: Demystifying the correlation between protein corona and aggregation phenomena, ACS Appl. Mater. Interfaces 14 (25) (2022) 28559–28569.
[20] Q. Han, Z.P. Candiloro, X. Cai, M. El Mohamad, B.P. Dyett, C.J. Rosado, J. Zhai, G. Bryant, C.J. Drummond, T.L. Greaves, Silica nanoparticle–protein aggregation and protein corona formation investigated with scattering techniques, ACS Appl. Mater. Interfaces (2025).
[21] F. Brunel, G. Billuart, P.-Y. Dugas, M. Lansalot, E. Bourgeat-Lami, V. Monteil, Crystallization of nanodomains in polyethylene latexes, Macromolecules 50 (24) (2017) 9742–9749.
[22] A. Thureau, P. Roblin, J. Pérez, BioSAXS on the SWING beamline at synchrotron SOLEIL, Appl. Crystallogr. 54 (6) (2021) 1698–1710.
[23] A. Guinier, La diffraction des rayons x aux très petits angles: Application à l'étude de phénomènes ultramicroscopiques, Ann. Phys. Onzieme Ser. 12 (1939) 161–237.
[24] L.R. Barbosa, M.G. Ortore, F. Spinozzi, P. Mariani, S. Bernstorff, R. Itri, The importance of protein-protein interactions on the pH-induced conformational changes of bovine serum albumin: a small-angle X-ray scattering study, Biophys. J. 98 (1) (2010) 147–157.
[25] F. Zhang, M.W. Skoda, R.M. Jacobs, R.A. Martin, C.M. Martin, F. Schreiber, Protein interactions studied by SAXS: Effect of ionic strength and protein concentration for BSA in aqueous solutions, J. Phys. Chem. B 111 (1) (2007) 251–259.
[26] I. Berndt, J.S. Pedersen, W. Richtering, Structure of multiresponsive "intelligent" core- shell microgels, J. Am. Chem. Soc. 127 (26) (2005) 9372–9373.

[27] I. Berndt, J.S. Pedersen, P. Lindner, W. Richtering, Influence of shell thickness and cross-link density on the structure of temperature-sensitive poly-n-isopropylacrylamide- poly-n-isopropylmethacrylamide core- shell microgels investigated by small-angle neutron scattering, Langmuir 22 (1) (2006) 459–468.
[28] I. Berndt, J.S. Pedersen, W. Richtering, Temperature-sensitive core–shell microgel particles with dense shell, Angew. Chem. 118 (11) (2006) 1769–1773.
[29] I. Langmuir, The adsorption of gases on plane surfaces of glass, mica and platinum, J. Am. Chem. Soc. 40 (9) (1918) 1361–1403.
[30] M. Schvartz, F. Saudrais, S. Devineau, J.-C. Aude, S. Chédin, C. Henry, A. Millán-Oropeza, T. Perrault, L. Pieri, S. Pin, et al., A proteome scale study reveals how plastic surfaces and agitation promote protein aggregation, Sci. Rep. 13 (1) (2023) 1227.
[31] H. Hahl, F. Evers, S. Grandthyll, M. Paulus, C. Sternemann, P. Loskill, M. Lessel, A.K. Husecken, T. Brenner, M. Tolan, et al., Subsurface influence on the structure of protein adsorbates as revealed by in situ X-ray reflectivity, Langmuir 28 (20) (2012) 7747–7756.
[32] S. Sarkar, S. Kundu, Structure and morphology of adsorbed protein (BSA) layer on hydrophilic silicon surface in presence of mono-, di-and tri-valent ions, JCIS Open 3 (2021) 100016.
[33] F. Brunel, P. Galanopoulo, E.E. Rodriguez, M. Lansalot, F. D'Agosto, In situ SAXS investigation of vinyl acetate polymerization-induced self-assembly, Polym. Chem. (2024).
[34] K.L. Prime, G.M. Whitesides, Self-assembled organic monolayers: Model systems for studying adsorption of proteins at aurfaces, Science 252 (5009) (1991) 1164–1167.
[35] W. Norde, C.E. Giacomelli, BSA structural changes during homomolecular exchange between the adsorbed and the dissolved states, J. Biotech. 79 (3) (2000) 259–268.
[36] M. Schvartz, Protéines en Contact avec des Macro et Microplastiques : Devenir en Solution et aux Interfaces (Ph.D. thesis), ED3MG, 2023.
[37] A. Kondo, S. Oku, K. Higashitani, Structural changes in protein molecules adsorbed on ultrafine silica particles, J. Colloid Interface Sci. 143 (1) (1991) 214–221.
[38] W. Norde, J.P. Favier, Structure of adsorbed and desorbed proteins, Colloids Surf. 64 (1) (1992) 87–93.
[39] W. Norde, C.E. Giacomelli, Conformational changes in proteins at interfaces: from solution to the interface, and back, in: Macromolecular Symposia, vol. 145, Wiley Online Library, 1999, pp. 125–136.
[40] L. Marichal, G. Klein, J. Armengaud, Y. Boulard, S. Chédin, J. Labarre, S. Pin, J.-P. Renault, J.-C. Aude, Protein corona composition of silica nanoparticles in complex media: Nanoparticle size does not matter, Nanomaterials 10 (2) (2020).
[41] J.K. Percus, G.J. Yevick, Analysis of classical statistical mechanics by means of collective coordinates, Phys. Rev. 110 (1958) 1–13.
[42] M.S. Wertheim, Exact solution of the percus-yevick integral equation for hard spheres, Phys. Rev. Lett. 10 (1963) 321–323.
[43] M. Teubner, R. Strey, Origin of the scattering peak in microemulsions, J. Chem. Phys. 87 (5) (1987) 3195–3200.
[44] P. Lindner, T. Zemb, Neutron, X-Rays and Light. Scattering Methods Applied to Soft Condensed Matter, in: North-Holland Delta, Elsevier Science, 2002.
[45] P. Debye, A. Bueche, Scattering by an inhomogeneous solid, J. Appl. Phys. 20 (6) (1949) 518–525.
[46] P. Debye, H. Anderson Jr., H. Brumberger, Scattering by an inhomogeneous solid. II. The correlation function and its application, J. Appl. Phys. 28 (6) (1957) 679–683.
[47] G. Brotons, Applicabilité de la Réflectivité de Neutrons et Rayons-x à l'étude de Films Minces de Polymères Nanocomposites (Ph.D. thesis), Le Mans, 2000.